INFORMATION TO USERS

This manuscript has been reproduced from the microfilm master. UMI films the text directly from the original or copy submitted. Thus, some thesis and dissertation copies are in typewriter face, while others may be from any type of computer printer.

The quality of this reproduction is dependent upon the quality of the copy submitted. Broken or indistinct print, colored or poor quality illustrations and photographs, print bleedthrough, substandard margins, and improper alignment can adversely affect reproduction.

In the unlikely event that the author did not send UMI a complete manuscript and there are missing pages, these will be noted. Also, if unauthorized copyright material had to be removed, a note will indicate the deletion.

Oversize materials (e.g., maps, drawings, charts) are reproduced by sectioning the original, beginning at the upper left-hand corner and continuing from left to right in equal sections with small overlaps. Each original is also photographed in one exposure and is included in reduced form at the back of the book.

Photographs included in the original manuscript have been reproduced xerographically in this copy. Higher quality 6" x 9" black and white photographic prints are available for any photographs or illustrations appearing in this copy for an additional charge. Contact UMI directly to order.

UMI

A Bell & Howell Information Company
300 North Zeeb Road, Ann Arbor MI 48106-1346 USA
313/761-4700 800/521-0600

The Zak Transform and a new Approach to Waveform Design

by

Irina Gladkova

A dissertation submitted to the Graduate Faculty in Mathematics in partial fulfillment of the requirements for the degree of Doctor of Philosophy, The City University of New York.

1998

This manuscript has been read and accepted by the Graduate Faculty in Mathematics in satisfaction of the dissertation requirement for the degree of Doctor of Philosophy.

January 26, 1998
Date

Chair of Examining Committee

January 26, 1998
Date

Executive Officer

Józef Dodziuk

José Moura

Burton Randol

Alphonse Vasquez

Supervisory Committee

THE CITY UNIVERSITY OF NEW YORK

Abstract

THE ZAK TRANSFORM AND A NEW APPROACH

TO WAVEFORM DESIGN

by

Irina Gladkova

Adviser: Professor José Moura

The ambiguity function $A_f(\tau, \nu)$ of a transmitted signal $f(t)$ measures the uncertainty with which the returning echo distinguishes, simultaneously, both ranges and velocities of a target system. For purposes of certain applications discussed in the engineering literature, $A_f(\tau, \nu)$ is desired to be thumbtack, i.e. a function whose absolute value has a graph with a strong peak at the origin, over a broad shallow base. The ambiguity function can be computed directly from the Zak transform $Z_f(x, y)$ of the signal $f(t)$ and so we propose to design a waveform in the Zak domain. A theorem that shows what properties the Zak transform of a signal should have for the ambiguity function to be thumbtack is derived and several new constructions based on this result are obtained. Furthermore, a simple method for the construction of generalized pulse train signals, whose Zak transforms are appropriately chosen trigonometric two-dimensional Chebyshev polynomials, is suggested, and applications to a multipath problem are considered. A multipath signal contains multiple returns of a transmitted signal, each is delayed and possibly

dilated. Detecting multipath signals using a standard engineering approach is prohibitively difficult because it is based on a multidimensional minimization problem. One way to avoid this optimization problem is to use a signal with a thumbtack ambiguity function. Then we suggest another way to overcome the difficulties of minimization which may be useful when there is a need to work with known, but not specially designed, signals. Our approach is based on simplifications of the minimization problem through increasing the dimension of the problem. Then, after the structure of our solution is studied, the continuous case is considered and a simple algorithm of a standard high frequency cutoff Fourier transform technique gives a 'smoothed out' solution of the original problem.

Acknowledgments

I wish I could thank my advisor, Professor Louis Auslander for providing stimulus, guidance and support. Unfortunately his sudden death did not let us finish this work together.

I would like to thank my thesis advisor, Professor José Moura for his help in the preparation of this work, for his patience and understanding.

I wish to thank Professor Burton Randol for his help and support throughout my graduate studies, from the very first day at the Graduate Center and especially during the last year. My life at the GC was enhanced by his friendship and advice.

I am very fortunate to have the love and support of my family. My parents' encouragement over my lifetime has ingrained in me the belief that I can accomplish anything I set out to do.

I would also like to thank my husband, Maxime Kudinov and my daughters, Eugenia and Ksenia for their love, support, patience and the sacrifices they have made these past $4\frac{1}{2}$ years.

This research was partially supported by DARPA under AFOSR contracts.

Contents

List of Figures

Chapter 1

Introduction.

The detection of the signals distorted by systems/channels with unknown and possibly time varying parameters has been a problem of critical importance in many applications, such as communications, radar, and sonar. In a wireless digital communications urban environment, the signal the mobile user receives consists of multiple delayed and scaled replicas of the signal the base station transmits due to reflection from surrounding obstacles and the mobility of the user. These types of propagation channels are called multipath channels [16]. A multipath channel is characterized by the delays, the attenuations, and the Doppler shifts associated with different replicas. These channel parameters are specific to the relative configuration of each sender-receiver pair. In general, they are not known and time-varying. In radar applications, the multipath effect is caused by reflections of radar signals from surrounding objects. The time delays and the Doppler shifts correspond to a target's range and velocity, respectively. In sonar, the multipath

signals result from surface and bottom reflections as well as refractive phenomena due to the nonhomogeneous ocean media.

The simplest received multipath signal model occurs when the transmitted signal is affected by a single type of distortion. A common example is the time delay signal model,

$$r(t) = s_K(t) + n(t) \tag{1.1}$$

$$= \sum_{k=1}^{K} \beta_k s(t - \tau_k) + n(t). \tag{1.2}$$

where s(t) is the transmitted signal, n(t) is additive noise, r(t) is the received signal and the signal parameters $\theta = \{K, \beta_k, \tau_k\}$ are unknown. Equation (1.2) can also be used in digital communications to model pulse amplitude modulated signals in the presence of jitter.

Doppler Effect: In radar and sonar, the detection problem is further complicated when detecting moving targets in a multipath environment. With wideband signals, the Doppler effect is caused by the target's motion compressing or expanding the transmitted signal, depending on whether the target is moving toward or away from the transmitter, respectively. In general, the received signal will be of the form

$$r(t) = s_K(t) + n(t) \tag{1.3}$$

$$= \sum_{k=1}^{K} \beta_k f(a_k t - \tau_k) + n(t). \tag{1.4}$$

where the change in scale, a_k, depends on the target's radial velocity and the delays, τ_k, depend on the target's range.

Under the narrowband assumption, the bandwidth of f in (1.4) is assumed much smaller than its central frequency, so that a Doppler effect on the received signal is approximated to be a pure frequency shift of the sent signal. Hence, using the exponential notation, the received signal with Doppler effect $r(t)$ can be modeled as sums of the translates and modulates of the sent signal $f(t)$,

$$r(t) = \sum_{k=1}^{K} \beta_k f(t - \tau_k) e^{-i\omega_k t} + n(t). \tag{1.5}$$

where now ω_k depends on the target's radial velocity and τ_k depends on the target's range.

Detecting signals with unknown, or nuisance, parameters is typically a two step process. First, maximum likelihood estimates of the unknown parameters are found. The estimates are then used to form a generalized likelihood ratio test. Shifts in time, frequency, and scale also occur in data transforms and are used to process the signals described above. For example, in the absence of multipath, i.e., $K = 1$, the peak of the cross-correlation function

$$R_{rs}(\tau) = \int_{-\infty}^{+\infty} r(t) s(t - \tau)\, dt.$$

provides a maximum likelihood estimate of the unknown delay τ in (1.2). Likewise, the peak of the narrowband ambiguity function,

$$A(\tau, \nu) = \int_{-\infty}^{+\infty} r(t) s(t - \tau) e^{-2\pi i \nu t}\, dt. \tag{1.6}$$

is the maximum likelihood estimate of the unknown delay and frequency shift of the transmitted signal when there is only a single received replica.

Similarly, the wideband ambiguity function,

$$W(a,\tau) = \int_{-\infty}^{+\infty} r(t)s(\frac{t-\tau}{a})\,dt. \tag{1.7}$$

is used for estimating delays and dilations.

We stress that the peaks of the cross correlation function and the ambiguity function represent maximum likelihood estimates only when one of the conditions below holds:

a. there is a single return.

b. the multiple returns are sufficiently separated in time, frequency or scale.

c. the sidelobes of the cross correlation and the ambiguity function are sufficiently smaller than the central spike, so they can not be confused with peaks corresponding to the time and frequency delays.

When the multipath signal violates these conditions, the estimate is found by minimizing the distance between the received signal and its model,

$$\min_{\theta} \|r(t) - s_K(t,\theta)\|. \tag{1.8}$$

where $s_K(t,\theta)$ is the parameterized multipath signal.

1.1 Main Contribution.

The central idea behind this research is to avoid the minimization problem (1.8) either by

i. designing signals whose ambiguity functions have a strong sharp peak at the origin over a sufficiently small base, or

ii. by applying the Fourier transform technique to a continuous version of equation (1.4) using known signals.

Designing signals with 'thumbtack' ambiguity functions is a special case of the more general issue of designing signals with a prescribed ambiguity function. The many attacks on this difficult problem ([23] p.125) since the publication of Woodward's book have yielded a great deal of insight into the nature of the ambiguity function (see [8]), but no solution to the general synthesis problem has been provided.

However, certain frequency-hop waveforms were found by Costas (see [9] or [10]) to have thumbtack-like ambiguity surfaces. The Costas waveform construction was algebraic, relying on the construction of matrices having special combinatorial properties. Our goal is to look at this problem using generalized pulse train signals that are generated by analytic, rather than algebraic, methods. As a tool for constructing such waveforms we use a Zak transform

$$Z_g(x,y) = \sum_{k=-\infty}^{\infty} g(x+k)e^{-2\pi iky}$$

which changes the formation of pulse trains

$$g(t) = \sum_{m,n} a_{mn} s(t-m) e^{2\pi i n t}$$

in the 'signal space' to multiplication

$$Z_g(x,y) = P(x,y) \cdot Z_s(x,y)$$

by a doubly-periodic function

$$P(x,y) = \sum_m \sum_n a_{mn} e^{2\pi i (nx+my)} \tag{1.9}$$

in 'Zak space'.

The significance of this for the problem of creating a particular ambiguity surface is that we may compute the ambiguity function (1.6) of g directly from Z_g :

$$A_g(\tau,\nu) = \int_0^1 \int_0^1 Z_g(x,y)\overline{Z_g(x+\tau, y+\nu)} e^{-2\pi i x\nu} dx\, dy. \tag{1.10}$$

If $s(t)$ is a pulse of duration 1, then $|Z_s(x,y)| = 1$ and we are led to consider two-dimensional trigonometric polynomials (1.9) as $Z_g(x,y)$ in (1.10). The study of geometric properties of a Zak transform for known waveforms with 'thumbtack' ambiguities gave us the idea to use Chebychev polynomials as candidates for $P(x,y)$.

Moreover, the volume property of the ambiguity function, which says that the volume under the surface must equal the square of the maximum, means that the ambiguities cannot be pushed down too much. For example attempts to nail the ambiguities on the integer lattice ([3, 5]), make them pop up in between the lattice. For signals whose Zak transforms are appropriately chosen trigonometric Chebychev polynomials in two variables, the ambiguities on the integer lattice-points in some region around the origin will be small, but not too small. This approach makes ambiguities smaller in between the integer lattice (due to the volume property).

In (3.3) we give a simple method for a construction of generalized pulse train signals, using Chebychev polynomials, and consider several such constructions.

A different way to overcome the difficulties of the minimization problem (1.8) may be needed when it is necessary to work with known, but not specially designed, signals. Then we may not have the advantages of signals with 'thumbtack' ambiguities, and the multiple returns may not be sufficiently separated in time or frequency.

Since among the parameters β_k, τ_k and K (see (1.1) and (1.2)) in the minimization problem (1.8) the coefficients β_k's are linear, choosing the τ_k's to be a partition of the (known in advance) interval $[T_0, T_1]$, we reduce this difficult non-linear multidimensional optimization problem to the linear one (the τ_k's and K are fixed now and the minimization is over parameters β_k).

The solution of this simplified problem is given by a matrix equation

$$\beta = S^{-1} \cdot \tilde{r}, \qquad \tilde{r} = (r(t), s(t - \tau_k))$$

of very large dimension - the price of the simplification. (Since we do not want to 'miss' any of the delays τ_k, the partition $\{\tau_k\}_{k=1}^{K}$ of the interval $[T_0, T_1]$ should be fine, which corresponds to large K. Those τ_k's that will have small attenuation coefficients β_k can be ignored in the sum (1.2)).

However the inversion of the matrix S of such large dimension need not be a problem. If the partition $\{\tau_k\}$ is chosen to be uniform, then the matrix S is of the symmetric Toeplitz type and can be inverted easily. The problem in this approach is of the following nature: by increasing the number of possible delays, we obtain a sum

$$s_K(t) = \sum_{k=1}^{K} \beta_k s(t - \tau_k)$$

which is so close to the received signal $r(t)$ that the distance

$$\|r(t) - s_K(t)\|_{L^2} = \|n(t)\|$$

is almost zero. This is not a contradiction of any kind, we were solving the problem

$$\min_{\tau_k, \beta_k, K} \|r(t) - s_M(t)\|_{L^2}$$

and we found a way to drive this distance (the norm of the noise) to zero. Since

there is no reason to suppose that this norm is in general extremely small, this makes it clear that in complete generality, the physical problem must contain additional features not considered in the standard approaches. However, when the noise is relatively small (in an easily defined sense) our method, as would be expected from the above remarks, gives excellent results. Moreover, we have found (cf. (4.5)) that refinements of our technique often give very satisfactory results even in the presence of large noise.

The analysis of the structure of the matrix S^{-1} shows that for the pulse of duration m as a sent signal $s(t)$ it can be approximated by

$$S^{-1} \approx (I - F^{-1})\Big((I - F^{m}) + (I - F^{-m})\Big)^{-1}(I - F).$$

where I is the identity matrix, F^{i} is a matrix with 1's on the upper ith diagonal and zeros everywhere else, and F^{-i} is a matrix with 1's on the lower ith diagonal and zeros everywhere else. This amounts to (difference) differentiation of a very oscillatory function $\tilde{r}$, which can be avoided with a high frequency cutoff Fourier transform technique.

1.2 Thesis Outline.

We now outline the chapters in this thesis.

In Chapter 2, first we present the definition and relevant properties of the Zak transform and the ambiguity function necessary for this work. Then, a few existing

techniques of radar waveform construction are explored in the context of waveform shaping with Zak transforms. These geometric properties, the idea of controlling the ambiguities on the integer lattice, and computing the ambiguity function in terms of the Zak transform, lead to a new way of constructing waveforms in the Zak domain which we present in Chapter 3.

In Chapter 3, we prove a theorem which, with a correct choice of certain parameters, provides control over the absolute values of the ambiguity function on the integer lattice and 'a bit' away from integer lattice points. Then we suggest a waveform design algorithm for constant amplitude signal with desired 'thumbtack-form' ambiguity function. Other thumbtack constructions are considered in this chapter based on two-dimensional trigonometric Chebyshev polynomials. More examples of this type are given in Appendix B. They all provide a desired ambiguity surface, the algorithm is very simple to implement and as the order of polynomial increases, the sidelobes of the ambiguity function are getting smaller.

In Chapter 4 we look at the multipath problem in a different way, i.e. not by designing a signal with a thumbtack ambiguity surface but working with a given, already known signal $s(t)$. First we simplify the difficult non-linear multidimensional optimization problem

$$\min_{\alpha_k, \tau_k, K} \|r(t) - \sum_{k=1}^{K} \alpha_k s(t - \tau_k)\|_{L_2}$$

to a linear minimization over parameters α_k. A solution of this simplified problem

is given by a matrix equation

$$\alpha = S^{-1} \cdot \tilde{r}.$$

which requires the inversion of a matrix S of large dimension. Then the approximation of the inverse matrix S^{-1} for different known signals are considered in order to see the structure of this matrix and, consequently, the character of the solution $\alpha = S^{-1}\tilde{r}$.

It is proven in theorem 4.1 that in this approach, the information about the multipath signal is in the (difference) derivative of the very oscillatory function $\tilde{r}$, which is why we suggest filtering out these oscillations with a Fourier transform technique. Continuous case is considered next, and after chopping off the high frequency components, the inverse Fourier transform gives a 'smoothed out' solution of the original problem.

Chapter 2

The Zak transform.

We first present the definition and relevant properties of the Zak transform. For a more thorough exposition, see [2, 13]. In particular, the facts stated in Section 2.1 about the Zak transform can be found in [13] and [2].

2.1 Definitions and notations.

The Zak transform of a given function $f(x)$ is defined as

$$Z_f(x, y) = \sum_{k=-\infty}^{+\infty} f(x+k)e^{-2\pi iky}. \tag{2.1}$$

We recognize in (2.1) the discrete Fourier transform of the sequence $f(x+k), k \in Z$. In this sense, the Zak transform is a mapping of a 1-dimensional function onto the 2-dimensional time-frequency plane. A similar object is also referred to as the Weil-Brezin mapping [4].

It will be convenient to use the following notation:

Translation: $(T_a f)(x) = f(x + a)$

Modulation: $(E_b f)(x) = f(x)e^{-2\pi ibx}$

Convolution: $(f * g)(x) = \int_{-\infty}^{+\infty} f(y)\overline{g(x - y)}\, dy$

Now, we have for $-\infty < a, b < \infty$ the formulas

$$Z_{T_a f}(x, y) = Z_f(x + a, y), \qquad -\infty < x, y < \infty \tag{2.2}$$

and

$$Z_{E_b f}(x, y) = e^{-2\pi ibx} Z_f(x, y + b), \qquad -\infty < x, y < \infty \tag{2.3}.$$

The formula (2.2) expresses the fact that a time translation of the signal over distance a is reflected by corresponding translation of Z_f in the time variable. The second formula has a similar interpretation, except for the factor $e^{-2\pi ibx}$.

The Zak transform satisfies the following periodicity relations. We have

$$Z_f(x + 1, y) = e^{2\pi iy} Z_f(x, y), \qquad -\infty < x, y < \infty \tag{2.4}$$

and

$$Z_f(x, y + 1) = Z_f(x, y), \qquad -\infty < x, y < \infty \tag{2.5}$$

Hence, Z_f is periodic in the frequency variable and quasiperiodic in the time variable. As a consequence, we have for integer n and m

$$Z_{E_m T_n f}(x, y) = e^{-2\pi imx + 2\pi iny} Z_f(x, y), \qquad -\infty < x, y < \infty \tag{2.6}$$

As a consequence of the periodicity relations (2.4) and (2.5), it is sufficient to consider the Zak transform on a unit square only.

Note that

$$f(x) = \int_0^1 Z_f(x, y)\, dy. \qquad -\infty < x < \infty. \tag{2.7}$$

Thus the mapping $f \rightarrow Z_f$ is invertible and f is continuous when Z_f is continuous. Again, see [13] for details.

Now, let S denote a square of the form $[0, 1] \times [0, 1]$. We have

$$\iint_S Z_f(x, y)\overline{Z_g(x, y)}dx\, dy = (f, g). \tag{2.8}$$

where the right-hand side is the usual inner product for square integrable functions. In particular, we have

$$\iint_S |Z_f(x, y)|^2 dx\, dy = \|f\|^2. \tag{2.9}$$

which shows that $f \rightarrow Z_f$ is an energy preserving transformation.

2.2 The Zak transform and the Ambiguity function.

Recognizing the importance of the ambiguity function as a signal design criterion in mathematical radar theory is generally credited to P. M. Woodward [23]. Further justification of its significance can be found in two works of W. Siebert [17, 18]. During the 1960s many properties of the ambiguity functions were established.

As references we cite [22], [20], and [21]. In this section we recall the definitions and results necessary for this work, cf. [8].

The cross-ambiguity function $A_{f,g}(\tau, \nu)$ of the signals $f(t)$ and $g(t)$ is given by

$$A_{f,g}(\tau, \nu) = \int_{-\infty}^{+\infty} f(t)\overline{g(t-\tau)}e^{-2\pi i\nu t}\, dt \tag{2.10}$$

and is defined for all values of the real variables τ and ν, which can be interpreted as time and frequency shift variables, respectively. Define the ambiguity function of a signal $f(t)$ by $A_f = A_{f,f}$. This function is also sometimes called the auto-ambiguity of f. It is proved in [22] that $A_f(\tau, \nu)$ is contained in the space $L^2(R^2)$ of all complex-valued functions $F(\tau, \nu)$ satisfying

$$\|F\|^2 = \int_{-\infty}^{+\infty}\int_{-\infty}^{+\infty} |F(\tau, \nu)|^2 d\tau\, d\nu < \infty \tag{2.11}$$

Moreover, if $A_f(\tau, \nu)$ is the ambiguity function of the signal $f(t)$, then:

a. $A_f(0, 0) = \|f\|^2$.

b. (maximum property) The largest value of the ambiguity function is always at the origin.

$$|A_f(\tau, \nu)| < A_f(0, 0). \qquad (\tau, \nu) \neq (0, 0).$$

c. Let $g(t) = s(t - x)e^{2\pi iyt}$, then $A_g(\tau, \nu) = A_s(\tau, \nu)e^{-2\pi i(x\nu + y\tau)}$,

d. (symmetry property) $A_f(\tau, \nu) = \overline{A_f(-\tau, -\nu)}$,

e. (volume property)

$$\int_{-\infty}^{+\infty}\int_{-\infty}^{+\infty} |A_f(\tau,\nu)|^2 d\tau\, d\nu = |A_f(0,0)|^2 = \|f\|^2.$$

Remark. The maximum property and the volume property strongly constrain the set of two-dimensional functions that can be ambiguity surfaces. The volume under the surface must equal the square of the maximum. Any attempt to push down the ambiguity function in one place makes it pop up somewhere else.

Note that the ambiguity function $A_f(\tau,\nu)$ of the signal $f(t)$ can be computed directly from the Zak transform $Z_f(x,y)$:

$$A_f(\tau,\nu) = \int_0^1\int_0^1 Z_f(x,y)\overline{Z_f(x+\tau,y+\nu)}e^{-2\pi i x\nu}dx\,dy.$$

As Woodward observed (see [23]), the ambiguity function $A_f(\tau,\nu)$ of a transmitted signal $f(t)$ measures the uncertainty with which the returning echo distinguishes, simultaneously, both ranges and velocities of a target system.

The uncertainty of information contained in a transmitted signal's echo is only one aspect of the signal design problem. More generally, the ambiguity function of a signal can be used as a tool to measure the signal's ability to perform certain tasks under given environmental conditions. The requirements can be expressed by some function $F(\tau,\nu)$ of time and frequency. For purposes of certain applications discussed in the engineering literature(see, for example, [19] p.418), $F(\tau,\nu)$ is desired to be thumbtack, i.e. a function whose absolute value has a graph with

a strong peak at the origin, over a broad shallow base. One of the possible applications of the signals with a thumbtack ambiguity function is in the multipath problems, as will be considered in chapter 4.

2.3 Waveform Shaping and Zak Transform.

We will now see that the Zak transform consolidates many current techniques of waveform construction into a simple form of multiplication of functions. In this thesis, we will call waveform shaping the replacement of the signal $s(t)$ by

$$g(t) = \sum_{m,n} a_{mn} s(t - m) e^{2\pi i n t}. \tag{2.12}$$

Many techniques of radar waveform construction fall under this general scheme.

Notice that

$$Z_g(x, y) = P(x, y) Z_s(x, y) \tag{2.13}$$

where

$$P(x, y) = \sum_{m,n} a_{mn} e^{2\pi i (nx + my)} \tag{2.14}$$

is a doubly-periodic function. So waveform shaping is multiplication by a doubly-periodic function under the Zak transform.

2.4 Frequency Hop Coding.

Frequency shift, or frequency hop coding, corresponds to waveform shaping of the following kind

$$g(t) = \sum_{n=0}^{N-1} \chi_{[0,1]}(t-n)e^{2\pi i\vartheta_n t}.$$

where ϑ_n is an integer depending on n. Frequently, one takes $\vartheta_1, \vartheta_2, \ldots, \vartheta_n$ to be a permutation of the integers $1, 2, \ldots, n$. Frequency hop coding is a waveform shaping with $a_{m,n} = 1$ for at most one n for each m, and $a_{m,n} = 0$ otherwise.

The Zak transform of this waveform is

$$Z_g(x,y) = \sum_{n=0}^{N-1} e^{2\pi i(ny-\vartheta_n x)} \qquad 0 \le x, y < 1. \tag{2.16}$$

Lemma. If $\vartheta = \vartheta_n$ is a permutation of $\{0, 1, \ldots, N-1\}$, then $Z_g(x,y)$ on $S = [0,1] \times [0,1]$ is a trigonometric polynomial with $N-1$ zeros on each side of the unit square S.

Proof. Note that

$$Z_g(x,0) = Z_g(x,1) = \sum_{n=0}^{N-1} e^{2\pi i\vartheta_n x} = \sum_{k=0}^{N-1} e^{2\pi ikx} = Z_g(0,y) = Z_g(1,y).$$

Thus it is enough to prove the statement for one side of the unit square. Now,

$$Z_g(0,y) = \sum_{n=0}^{N-1} e^{2\pi iny} = 1 + w + \ldots + w^{N-1} = (w-a)(w-a^2)\ldots(w-a^{N-1}).$$

where $w = e^{2\pi iy}$ and $a = e^{2\pi i/N}$. Therefore $Z_g(x, y)$ has $N - 1$ zeros on each side of the unit square.

Note that $Z_g(0,0) = Z_g(0,1) = Z_g(1,0) = Z_g(1,1) = \sum_{n=0}^{N-1} 1 = N$. The shape of the absolute value of Z_g on the boundary of the unit square is shown on figure (2.1).

Remark: The function $\sum_{n=0}^{N-1} e^{2\pi iny}$ is well known in the engineering literature where it is refered to as the discrete $sinc$ function.

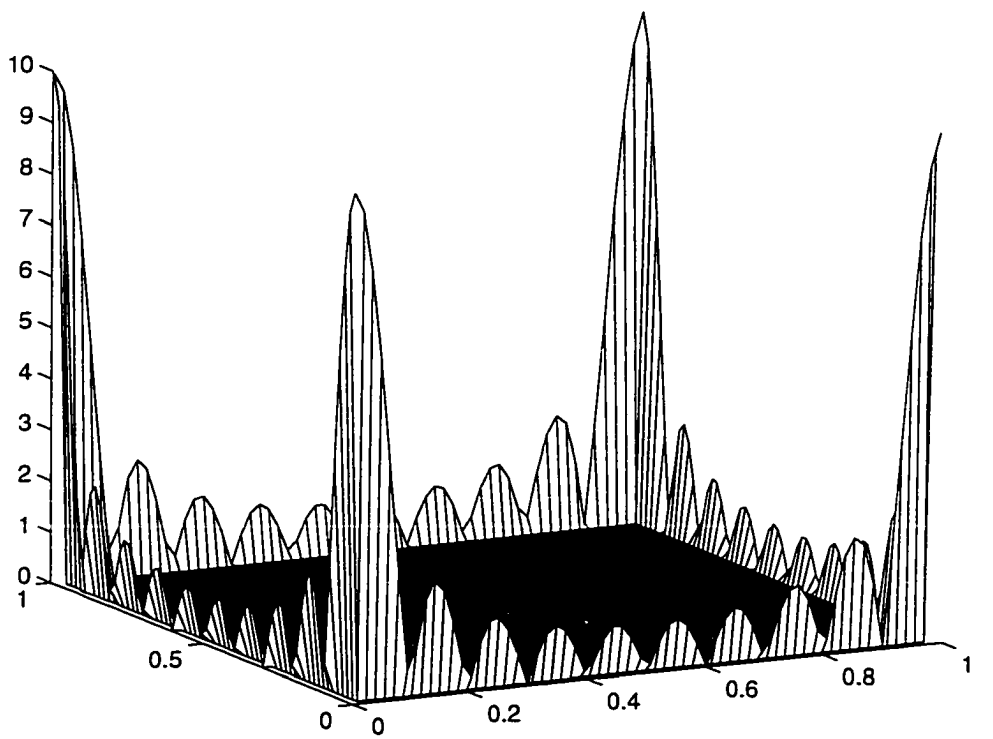

Figure 2.1. The shape of the Zak transform on the boundary of S.

2.5 Ambiguity on the Integer Lattice.

Definition: An ambiguity function A_f with $A_f(0,0) = 1$, is *lattice-thumbtack* with parameter ϵ, if $|A_f(m,n)| < \epsilon$, for all $(m,n) \neq (0,0)$.

To understand which f might have the above property, consider the ambiguity function on the integer lattice in terms of the Zak transform.

$$A_f(n,m) = \int_0^1 \int_0^1 Z_f(x,y)\overline{Z_f(x+n,y+m)}e^{2\pi imx}dx\,dy$$

$$= \int_0^1 \int_0^1 |Z_f(x,y)|^2 e^{2\pi i(mx+ny)}dx\,dy$$

Thus the $A_f(n,m)$'s are the Fourier coefficients of the real, non-negative function $|Z_f(x,y)|^2$.

Obviously, if $|Z_f(x,y)| = 1$ then the signal $f(t)$ has a lattice-thumbtack ambiguity function. The trivial example of such signal is a rectangular pulse of duration 1:

$$s(t) = \begin{cases} 1, & 0 \leq t \leq 1, \\ 0, & \text{otherwise.} \end{cases}$$

$Z_s(x,y) \equiv 1$, for $0 \leq x, y \leq 1$, and

$$A_s(m,n) = \begin{cases} 1, & n = m = 0, \\ 0, & \text{otherwise.} \end{cases}$$

A non-trivial example of a signal with lattice-thumbtack ambiguity function will be considered in section 3.3.

2.6 Zak transform of some known waveforms.

In this section we want to consider some of the existing techniques of radar waveform construction to see the geometric properties of the Zak transform. These known techniques can be found in the references [8], [9],[10],[11], and [15].

2.6.1 Costas Arrays.

Costas [9] suggested that, under the scheme of frequency hop coding, if we choose the permutation ϑ cleverly, we can get a waveform with good thumbtack-like ambiguity properties. Discussion beyond the original paper on Costas arrays can be found in [8],[10], and [11].

To design a Costas Array, ϑ is chosen so that no two pairs of terms in the sum will have the same shift in both time and frequency.

Definition: A Costas array **A** is an N-by-N array of 0's and 1's such that

$$\sum_{i=0}^{N-1} A_{ij} = \sum_{j=0}^{N-1} A_{ij} = 1.$$

$$\sum_{i=0}^{N-1}\sum_{j=0}^{N-1} A_{ij}A_{i+r,j+s} \leq 1. \quad if \quad r \neq 0, s \neq 0.$$

(with the understanding that $A_{i+r,j+s} = 0$ if either $i + r$ or $j + s$ is not in the set of indices 0,1,...,N-1).

It is convenient to represent the $N \times N$ permutation matrix **A** on an $N \times N$ grid, with a dot in the middle of cell (i, j) if and only if $A_{ij} = 1$. The Costas condition then says that the $(N^2 - N)/2$ lines connecting pairs of distinct dots are

all different as vectors; that is, no two of these lines are equal in both length and slope.

General rules for constructing or classifying Costas arrays are not known, but several constructions are known for special cases. A simple construction is available when $N + 1$ is a prime. Let p be a prime and $N = p - 1$, and let α be a primitive element of the integer arithmetic system modulo p. An N by N Welch-Costas array is an N by N array of 0's and 1's such that $A_{ij} = 1$ if and only if $j = \alpha^i$. For example, with $p = 7$ and the primitive element $\alpha = 3$ the permutation $v = [3\ 2\ 6\ 4\ 5\ 1]$ (see [8]).

Let us consider the Welch-10 and Welch-30 codes as the examples of Welch-Costas arrays (see [10]). The sequence v =[1 3 7 4 9 8 6 2 5 0] is a Welch-10 permutation and the signal corresponding to the Welch-10 code is given on figure (2.2). Cf. [10].

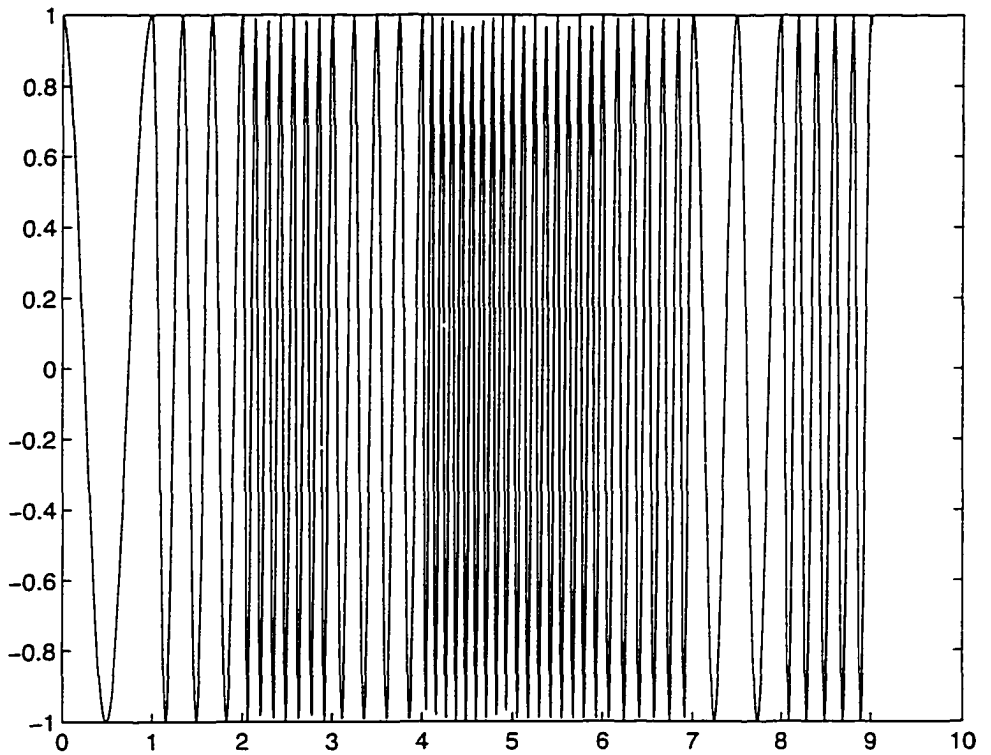

Figure 2.2. Signal corresponding to the Welch-10 Costas Array.

The sequence v =[2 8 26 18 25 15 16 19 28 24 12 7 23 9 29 27 21 3 11 4 14 13 10 1 5 17 22 6 20 0] is a Welch-30 permutation, cf. [10]. The Zak transforms of the Welch-10 and Welch-30 waveforms are given in figures (2.3) and (2.4).

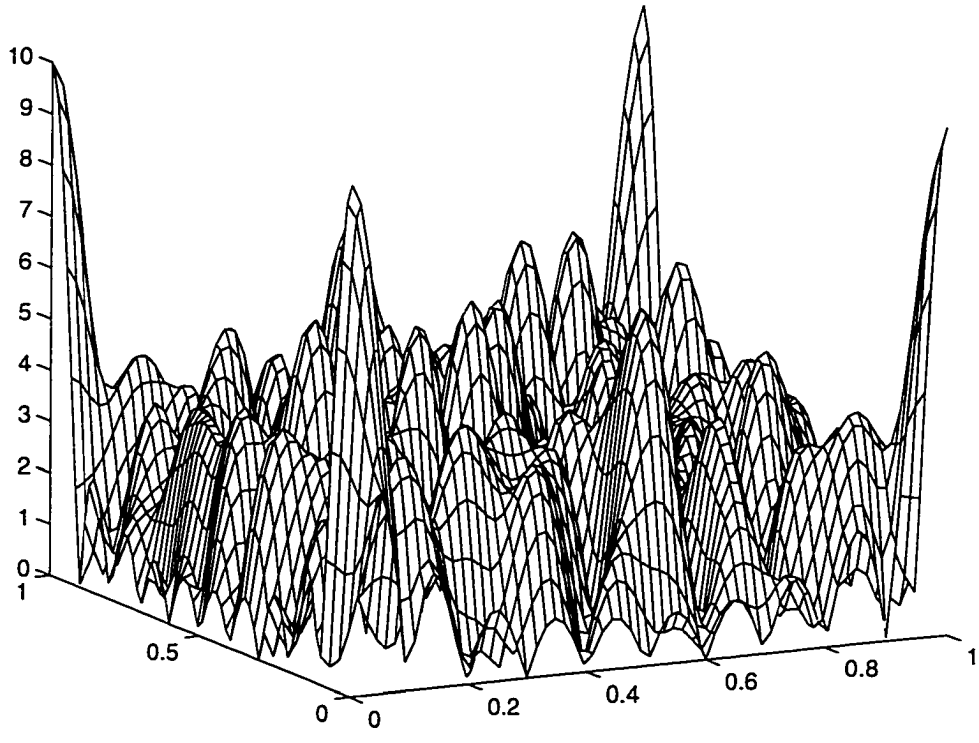

Figure 2.3. The Zak transform of the Welch-10 Waveform.

The Zak transforms of these codes have interesting properties. If we graph their absolute values over a unit square, the graph has four peaks of equal height at the vertices of the square, while in the part of the square away from the vertices, the graph is of relatively small height.

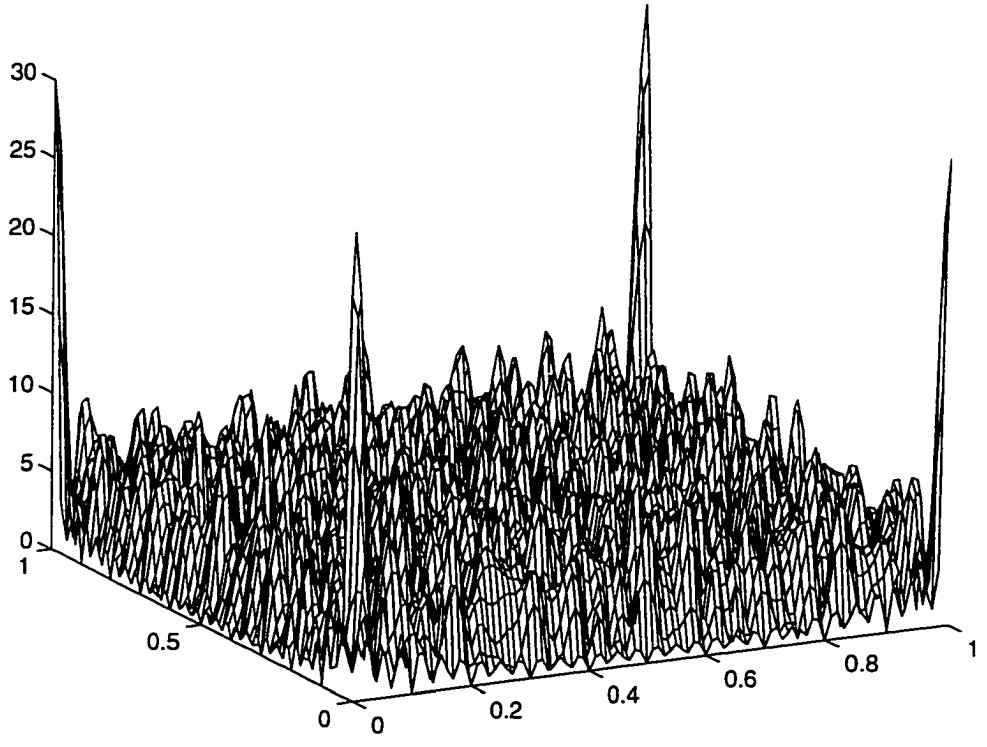

Figure 2.4. The Zak transform of the Welch-30 Waveform.

The ambiguity surface of the signal corresponding to the Welch-30 code is given on figure (2.5). It has a desired thumbtack shape.

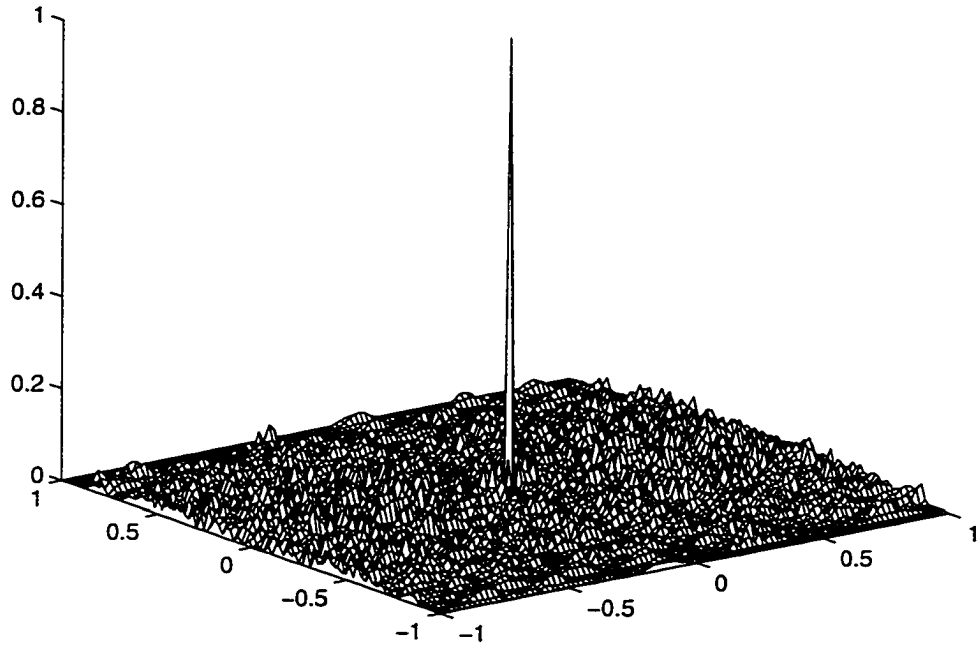

Figure 2.5. The Ambiguity surface of the Welch-30 waveform.

2.6.2 Multiple access frequency hopping patterns.

Mersereau and Seay [15] suggested a different approach for constructing frequency-hopping sequences. Their technique produces Q^{k-1} hopping patterns, each of which is periodic with period $Q-1$, where Q is the number of available frequencies and k is the maximum number of hits per period that can occur between any pairs of patterns, or any pattern and a constant frequency signal, for any relative time and frequency shifts between those patterns. For definitions of terms used in

this section, see [15]. Two examples of such patterns with $Q = 23$ and $k = 3$ are given below. They are generated from the equation

$$v = nG,$$

where

$$G = \begin{pmatrix} 1 & 1 & 1 \ldots & 1 \\ 5 & 5^2 & 5^3 \ldots & 5^{22} = 1 \\ 5^2 & 5^4 & 5^6 \ldots & 1 \\ 5^3 & 5^6 & 5^9 \ldots & 1 \end{pmatrix}.$$

$n = [0, 1, X, Y], X, Y \in 0, 1, 2, \ldots, 22.$

The pattern $v^1 = [5, 5^2, 5^3, \ldots 5^{22} = 1]$, taken mod 23, is

[5, 2, 10, 4, 20, 8, 17, 16, 11, 9, 22, 18, 21, 13, 19, 3, 15, 6, 7, 12, 14, 1]

is generated by $n = [0, 1, 0, 0]$ and the pattern v^2 generated by $n = [0, 1, 1, 0]$,

$v^2 = [5 + 5^2, 5^2 + 5^4, 5^3 + 5^6, \ldots 5^{22} + 5^{44} = 2]$

$= [7, 6, 18, 20, 6, 3, 7, 19, 17, 21, 0, 20, 2, 21, 12, 12, 10, 19, 10, 18, 3, 2]$.

By inspection we see that neither of these particular waveforms uses any chip frequency more than twice.

The Zak transforms of the signals corresponding to these frequency-hopping patterns are given in figures 2.6 and 2.7.

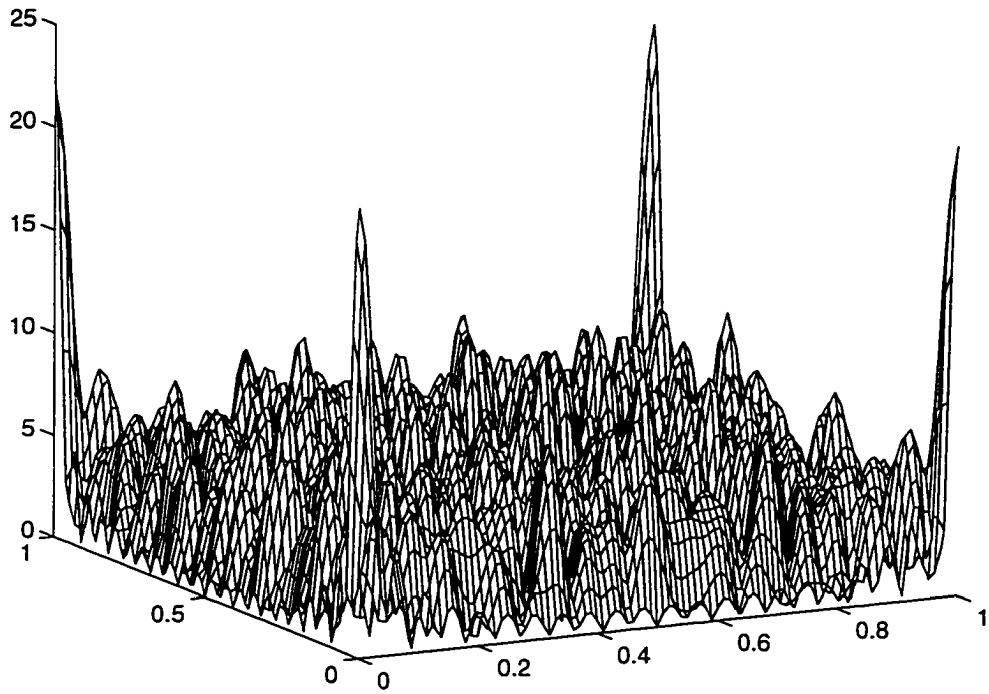

Figure 2.6. The Zak transform of the waveform generated by $n = [0.1.0.0]$.

The absolute value graphs of the Zak transforms, as can be seen from figures 2.6 and 2.7, have the shape described above: four peaks at the vertices of the unit square and relatively small height on the rest of the square.

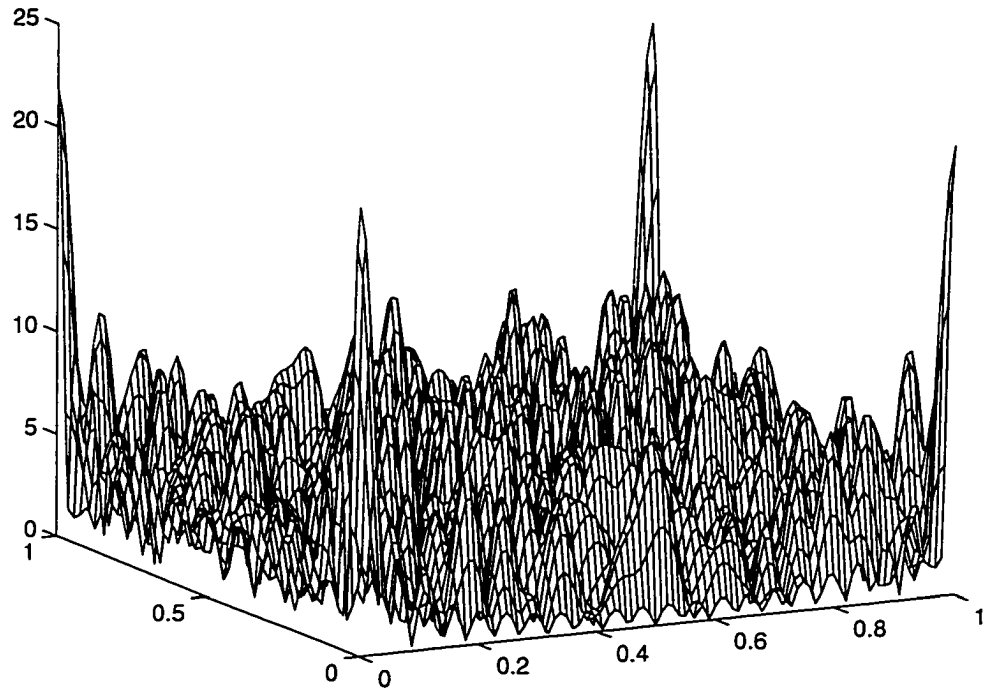

Figure 2.7. The Zak transform of the waveform generated by $n = [0, 1, 1, 0]$.

The closeup of the ambiguity surface is given on figure 2.8.

The magnitude of the ambiguity function is less than 0.097 outside the central region. The maximum magnitude of the central region, exclusive of the main lobe, is 0.35.

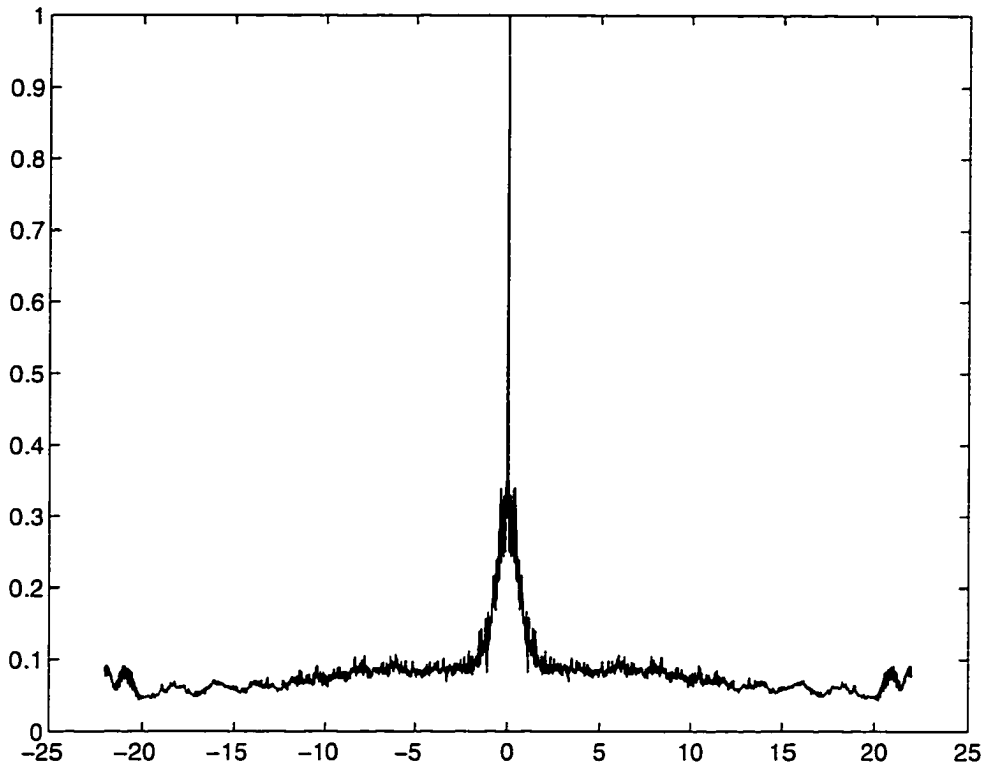

Figure 2.8. The closeup of the ambiguity surface.

These geometric properties suggest a new way of constructing waveforms in the Zak domain.

Chapter 3

New Thumbtack Construction

3.1 Main theorem

Set $\mathbf{K}= S - \bigcup_{0\le i,j\le 1} B_\epsilon(i,j)$, where $B_\varepsilon(i,j)$ is the open ball of radius ε about the point (i,j), S is a square $[0,1]\times[0,1]$. In other words, $\mathbf{K}$ is the unit square with cut off corners.

Let $\tau = n+\eta, \nu = m+\xi$, where n, m are integers and $0 < \eta, \xi < 1$.

Theorem 3.1. If $Q(x,y)$ is a nonnegative, square-integrable, real valued function defined on S with Fourier coefficients

$$b_{nm} = \int_0^1 \int_0^1 Q(x,y) e^{2\pi i(mx+ny)} dx\, dy, \tag{3.1}$$

such that

$$b_{00} = 1, \qquad |b_{nm}| < \varepsilon_1, \qquad n, m \neq 0 \tag{3.2}$$

and

$$Q(x,y) < \varepsilon_2 \qquad \text{for } (x,y) \in \mathbf{K} \tag{3.3}$$

Then $|A_s(\tau,\nu)| < \delta$ for $\eta,\xi = 0$(i.e. τ,ν are integers) and $2\varepsilon < \eta,\xi < 1-2\varepsilon$, where $s(t) = Z^{-1}\left(\sqrt{Q(x,y)}\right)(t)$, $\delta = \max(\varepsilon_1, \varepsilon_2 + 2\pi\varepsilon^2\sqrt{\varepsilon_2}M)$, $M = Q(0,0)$.

Remark. The appropriate choice of ε_1 and ε_2 provides control over the absolute values of the ambiguity function on the integer lattice and at least 2ε away from integer lattice-points. If ε is small enough this provides the desired degree of control.

Proof. First let us show that $|A_s(\tau,\nu)| < \delta$ for $\eta,\xi = 0$, i.e. for τ,ν-integers.

Now

$$A_s(n,m) = \int_0^1 \int_0^1 |Z_s(n,m)|^2 e^{2\pi i(mx+ny)}\,dx\,dy$$

$$= \int_0^1 \int_0^1 Q(x,y) e^{2\pi i(mx+ny)}\,dx\,dy = b_{nm},$$

since $Z_s(x,y) = \sqrt{Q(x,y)}$.

Therefore $|A_s(n,m)| = |b_{nm}| < \varepsilon_1 \le \delta$.

Next we show that $|A_s(\tau,\nu)| < \delta$, for $2\varepsilon < \eta,\xi < 1-2\varepsilon$. Now

$$A_s(\tau,\nu) = \int_0^1 \int_0^1 Z_s(x,y)\overline{Z_s(x+\tau,y+\nu)} e^{-2\pi i\nu x}\,dx\,dy =$$

$$= \int_0^1 \int_0^1 Z_s(x,y)\overline{Z_s(x+\eta,y+\xi)} e^{2\pi i(nx+my)} e^{-2\pi i\xi x}\,dx\,dy.$$

Thus,

$$|A_s(\tau,\nu)| \leq \int_0^1 \int_0^1 |Z_s(x,y)| \cdot |Z_s(x+\eta, y+\xi)| dx\, dy$$

$$\leq (1-2\pi\varepsilon^2)\varepsilon_2 + 2\pi\varepsilon^2\sqrt{\varepsilon_2}M \leq \delta.$$

3.2 Waveform design algorithm.

To apply Theorem 3.1, we need a nonnegative, real-valued function $Q(x,y)$ satisfying the conditions (3.2), (3.3). We prescribe nonnegative uniformly distributed random values on a discrete grid approximating $\mathbf{K}$, and appropriately large values on the corners of $S - \mathbf{K}$ (figure (3.1)). This makes $Q(x,y)$ chaotic and bounded by some small constant on $\mathbf{K}$ and large in the corners. In general, the Fourier coefficients, due to the randomness, will be small and thus the ambiguity function of the signal $s(t) = Z^{-1}(\sqrt{Q(x,y)})$ by the theorem, will be thumbtack. Figure (3.2) is the ambiguity surface on the integer lattice.

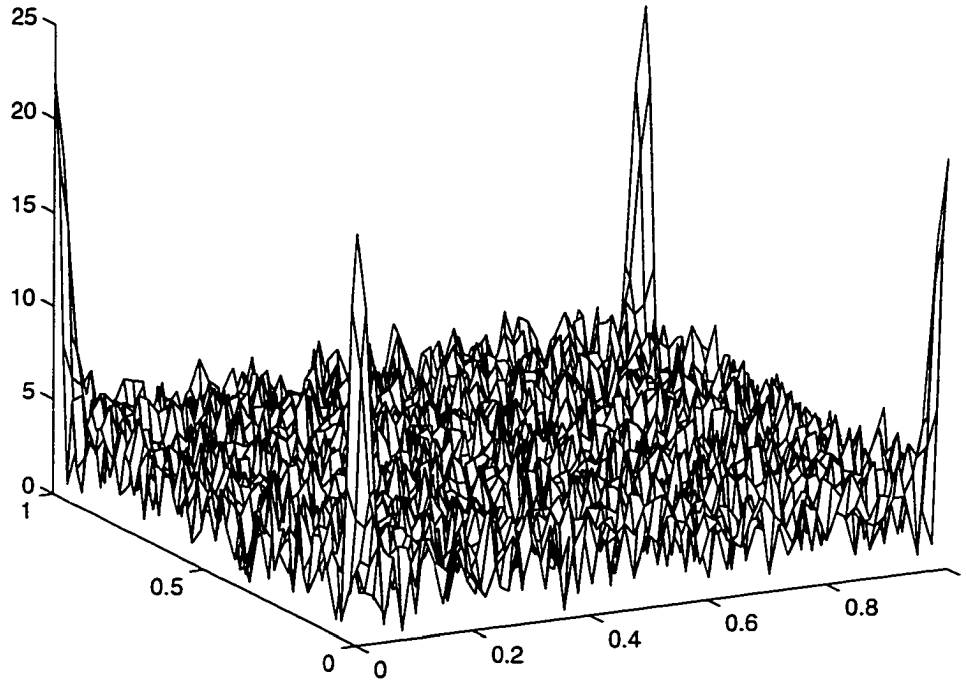

Figure 3.1. The magnitude of the Zak transform.

Unfortunately, the signal $s(t) = Z^{-1}(\sqrt{Q(x,y)})$ is not 'nice' in the 'signal space'. It is not, for example, of the form (2.12). To make it so, let us approximate $\sqrt{Q(x,y)}$ by a trigonometric polynomial of order 33

$$\sqrt{Q(x,y)} \approx P(x,y) = \sum_{n,m=1}^{33} a_{nm} e^{2\pi i(mx+ny)}.$$

where the a_{nm}'s are the Fourier coefficients of $\sqrt{Q(x,y)}$.

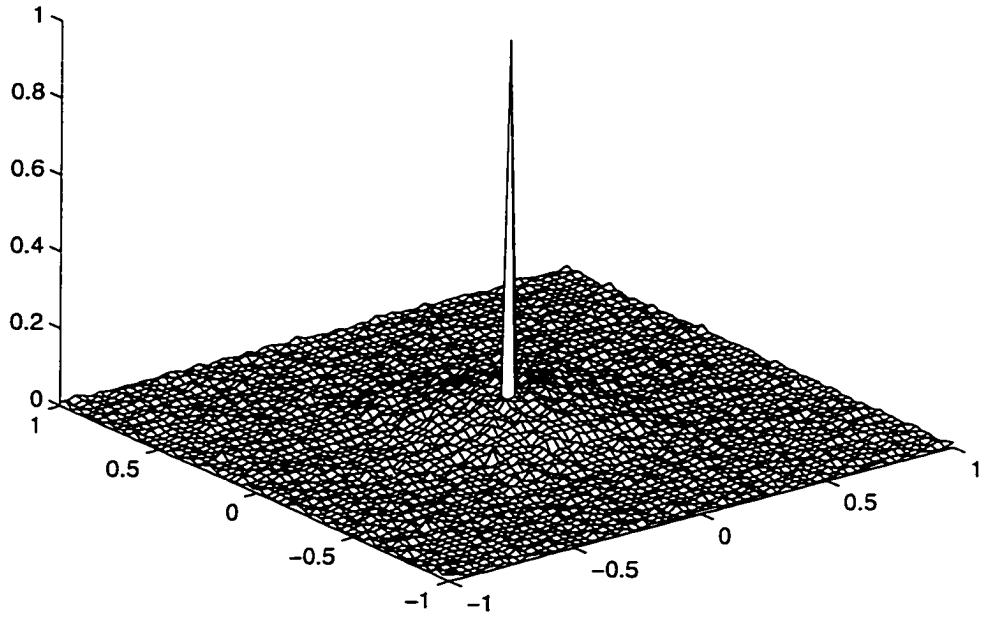

Figure 3.2. Ambiguity function on the integer lattice.

The absolute value of the polynomial $P(x, y)$ is shown in figure (3.3) and the ambiguity function on the integer lattice is shown in figure (3.4).

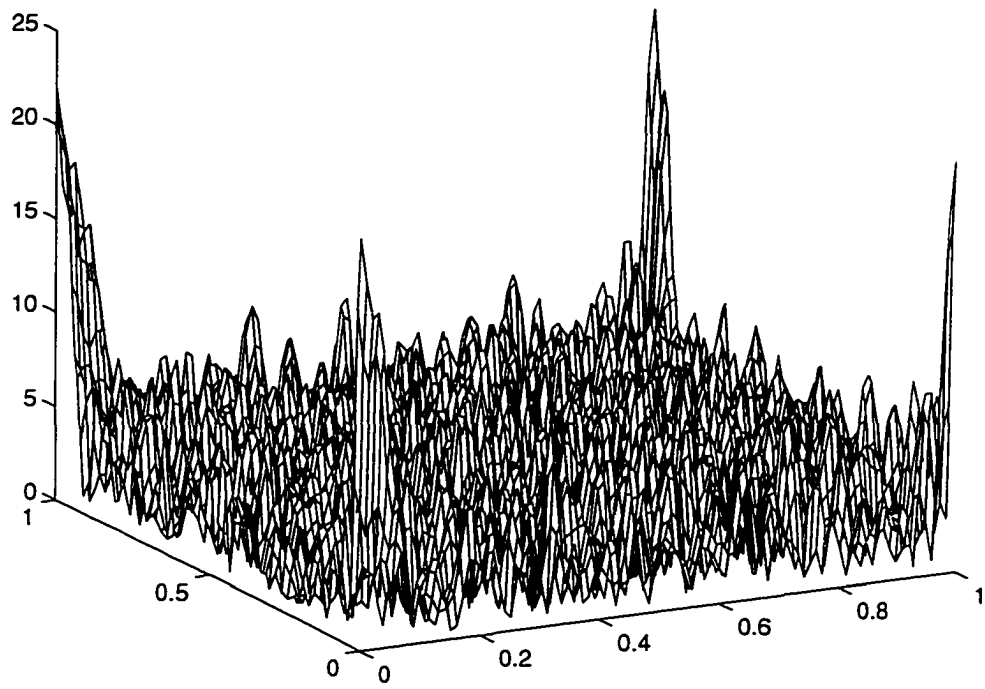

Figure 3.3. $|P(x, y)|$ - polynomial approximation in the Zak domain.

The magnitude of the actual ambiguity function is given in figure (3.5) and the real part of the signal

$$s(t) = \sum_{n,m=1}^{33} a_{nm} \chi_{[0,1]}(t - n) e^{2\pi i m t}$$

with matrix $A = \{a_{nm}\}$ of the size 33×33 is shown in figure (3.6).

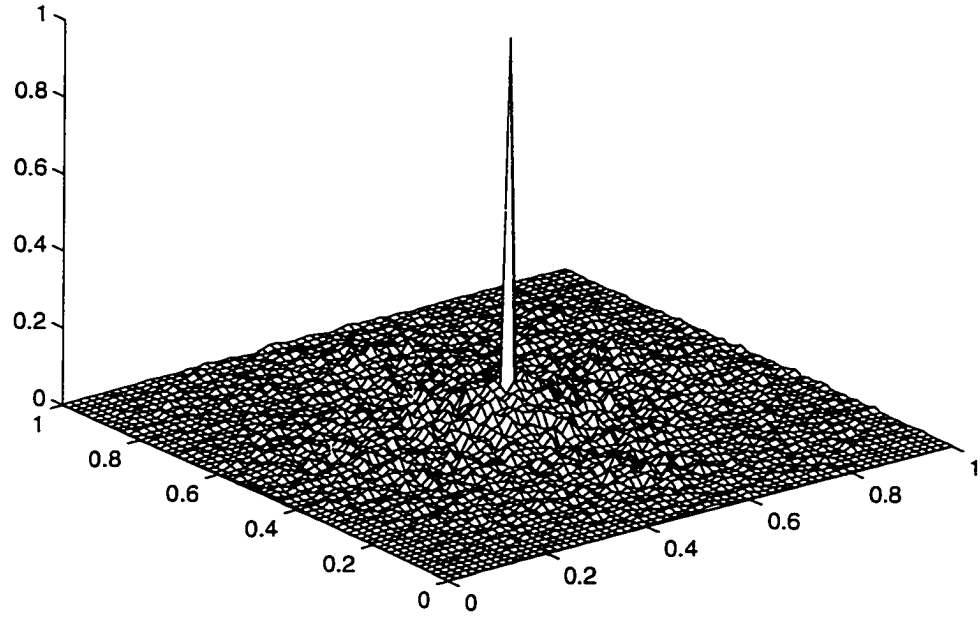

Figure 3.4. Ambiguity function of the polynomial approximation on the integer lattice.

The signal $s(t)$ so obtained is not good for radar purposes since its amplitude is not constant. To make $s(t)$ better for radar purposes, let us consider the signal $f(t) = e^{i\vartheta_s(t)}$, where $\vartheta_s(t)$ is the phase of the signal $s(t)$.

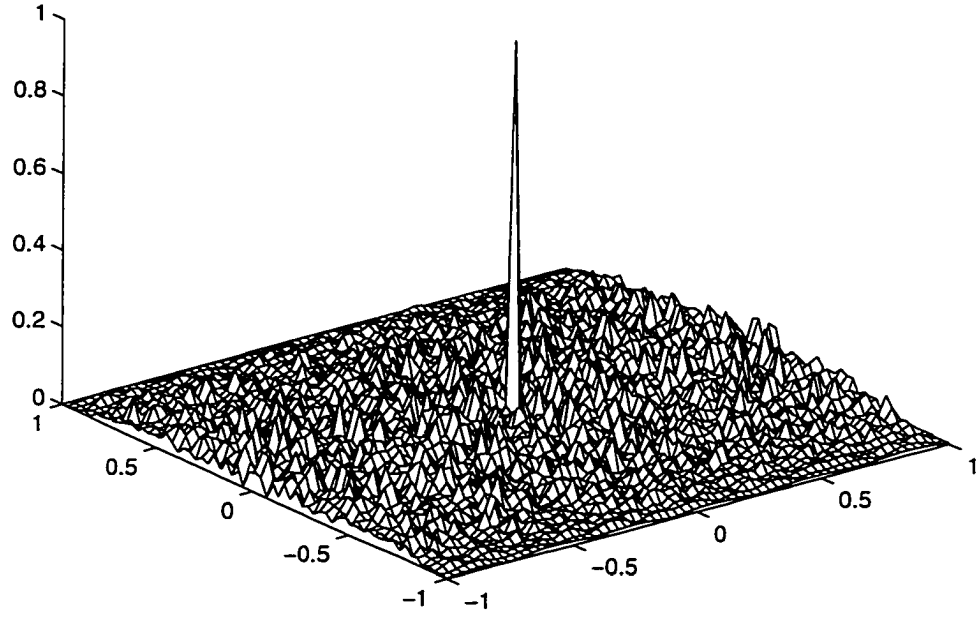

Figure 3.5. The magnitude of the actual ambiguity function.

The closeup of the ambiguity surface of the signal $f(t)$ with constant amplitude and the same phase as $s(t)$ is shown on figure (3.7). It also has the thumbtack shape.

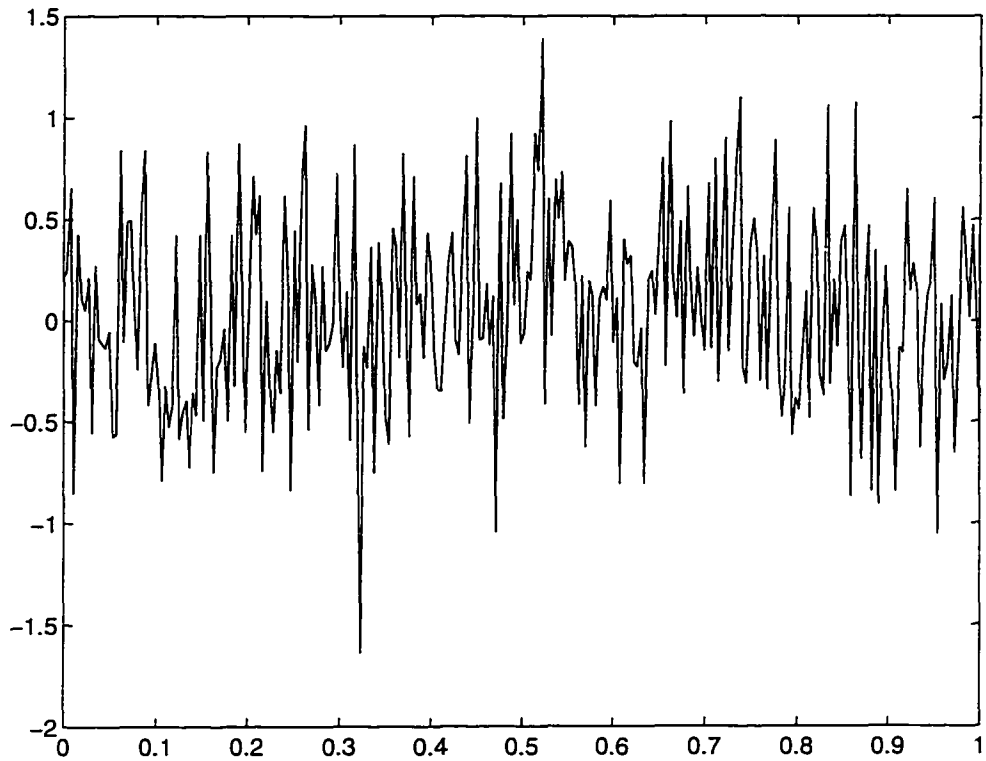

Figure 3.6. The real part of the signal.

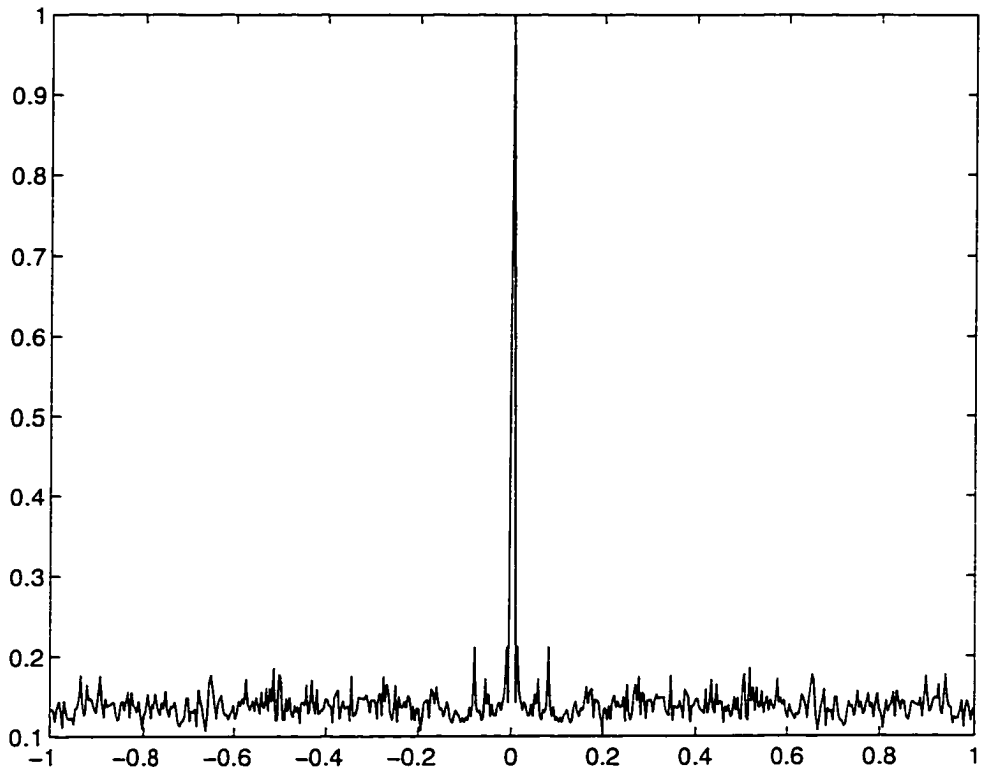

Figure 3.7. The closeup of the ambiguity surface of the signal $f(t) = e^{i\theta_s(t)}$.

3.3 The thumbtack construction based on Chebyshev polynomials.

Another type of function that fits the conditions of theorem 3.1 can be obtained from Chebyshev polynomials [1]

$$T_k(x) = \cos(k \arccos(x)) \tag{3.4}$$

in the following manner.

We will choose as candidates for $Q(x,y)$ functions of the form

$$C_k(x,y) = \lambda T_k(\varphi(x,y)), \tag{3.5}$$

where $\lambda > 0$ and $\varphi(x,y)$ is a suitably chosen trigonometric polynomial in two variables.

The properties of $C_k(x,y)$ are as follows: it is bounded by λ in the domain $K_0 = \{(x,y) : |\varphi(x,y)| < 1\}$ and it grows fast in the domain $K_\infty = \{(x,y) : |\varphi(x,y)| > 1\}$ (the growth, obviously, depends on the parameter k). Thus the condition (3.3) of the theorem is satisfied with the appropriate choice of $\varphi(x,y)$. One of the possible examples is

$$\varphi(x,y) = \cos \pi x \cdot \cos \pi y \tag{3.6}.$$

The polynomial $C_{40}(x,y) = e^{0.04} T_{40}(\cos \pi x \cdot \cos \pi y)$ is shown on figure (3.8).

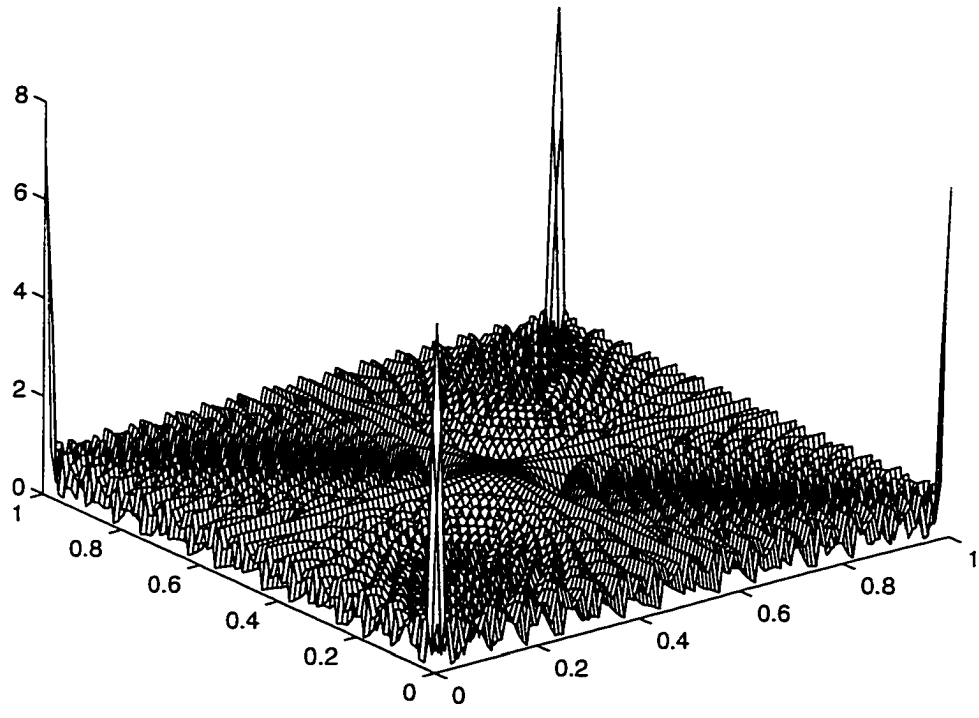

Figure 3.8. Zak transform of the new construction based on Chebyshev polynomials.

The next step is to find the corresponding function in 'signal space' . Due to Theorem 3.1,

$$s(t) = Z^{-1}\left(\sqrt{C_{40}(x,y)}\right).$$

Since

$$T_k^2(\varphi(x,y)) = \frac{1}{2}\left(T_{2k}(\varphi(x,y)) + 1\right)$$

$\sqrt{C_{40}(x,y)}$ is an even trigonometric polynomial, that can be written as $\sum b_{nm} e^{2\pi i(mx+ny)}$.

where $B = \{b_{nm}\}$ is a symmetric matrix with real b_{nm}. Therefore the signal

$$s(t) = \sum_{n,m} b_{nm} \chi_{[0,1]}(t-n) e^{2\pi i m t}$$

is also real.

The signal, corresponding to the $C_{20}(x, y)$ is shown in figure (3.9).

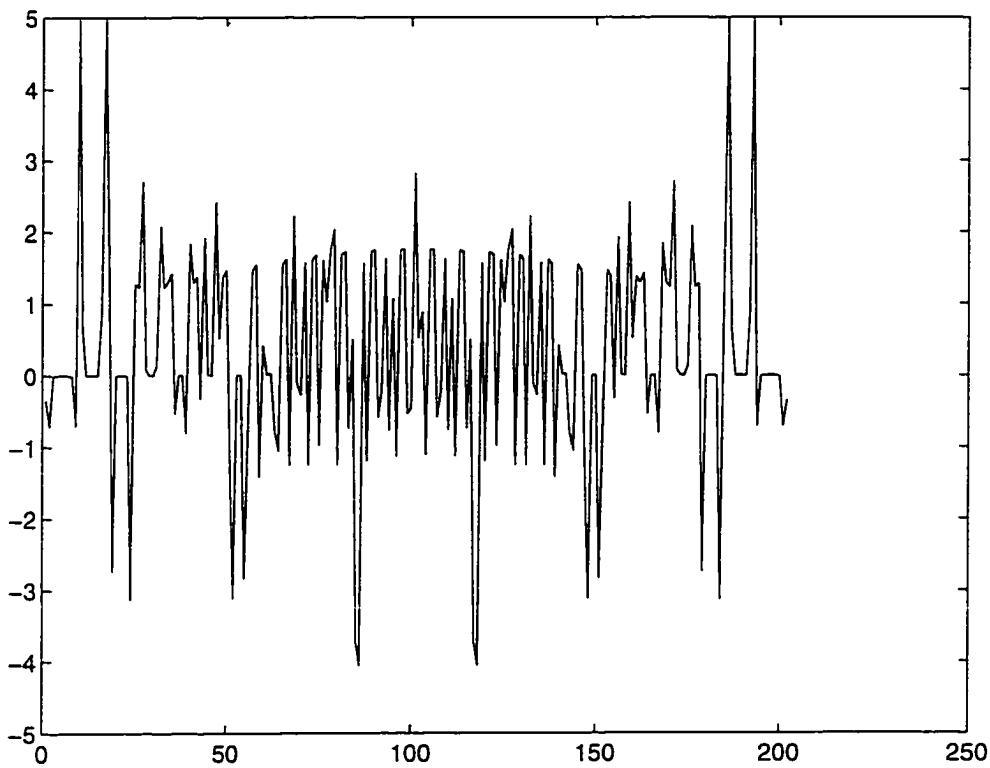

Figure 3.9. Signal corresponding to the $C_{20}(x, y)$.

The ambiguity on the integer lattice is shown in figure 3.10. We should note at this point that in practice, one is not interested in resolving targets at all ranges, and those parts of the ambiguity diagram which are remote from the origin (in

any direction) are of no practical interest. So, in designing signals with thumbtack ambiguity function, we may usually draw a circle around the origin and try to push the ambiguities outside it.

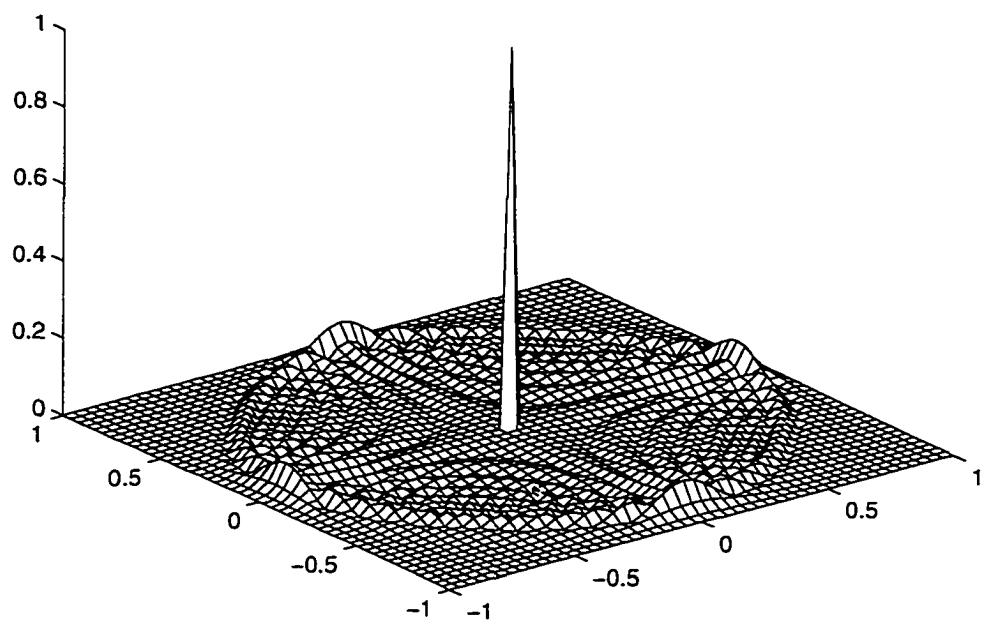

Figure 3.10. Ambiguity function on the integer lattice.

When dealing with signals whose Zak transform is generated by Chebyshev polynomials, we automatically achieve the effect of pushing ambiguities out of the origin on the integer lattice since the ambiguity function on the integer lattice equals the Fourier coefficients of the Chebychev polynomial. This approach makes ambiguities smaller in between the integer lattice (due to the volume property of

ambiguity functions). The magnitude of the actual ambiguity function is shown in figure 3.11.

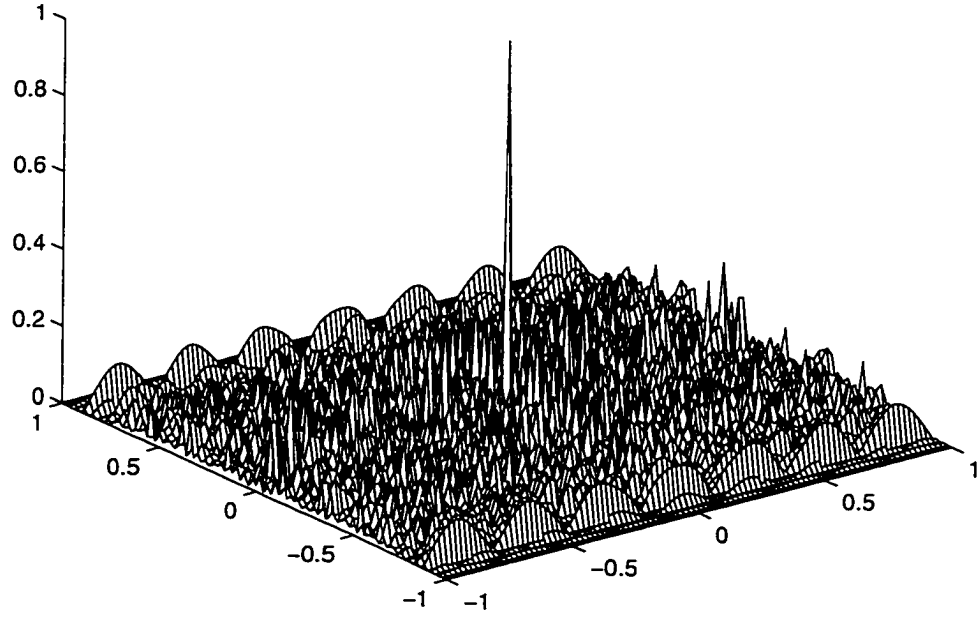

Figure 3.11. Magnitude of the actual ambiguity function.

More examples of this type are given in Appendix B.

Chapter 4

The multipath problem

4.1 Multipath based on linear transforms

Assume that the sent signal $s(t)$ is known and the multipath signal is produced from a linear combination of delayed replicas

$$s_K(t) = \sum_{k=1}^{K} \alpha_k s(t - \tau_k). \tag{4.1}$$

The received signal $r(t)$ is

$$r(t) = s_K(t) + n(t). \tag{4.2}$$

where $n(t)$ is Gaussian white noise. The number of replicas K, the attenuation coefficients $\{\alpha_k\}$ and the delays $\{\tau_k\}$ are all unknown. For a known signal $s(t)$, detecting the presence of $s_M(t)$ with a generalized maximum likelihood test

receiver requires calculating an estimate $s^*_{K^*}(t)$ of $s_{K^*}(t)$ by finding those parameters $K^*, \{\alpha^*_k\}, \{\tau^*_k\}$. that minimize the distance

$$\|r(t) - \sum_{k=1}^{K} \alpha_k s(t - \tau_k)\|_{L^2} \tag{4.3}$$

which is, generally speaking, a difficult multidimensional optimization problem.

However, if the $\{\tau_k\}$ are known to be in the interval (T_0, T_1). the sequence $\{\tau_k\}$ of unknown delays can be taken as a partition of the interval (T_0, T_1). Thus, the τ_k's and K are now fixed and the optimization problem (4.3) is reduced to the minimization over the parameters α_k.

There is a price to pay for this simplification - the partition $\{\tau_k\}$ should be fine, which corresponds to large K. Those τ_k's with corresponding small attenuation coefficients α_k can be ignored in the sum (4.1).

By differentiating (4.3) with respect to α_k

$$\frac{\partial}{\partial \alpha_k}\Big(r(t) - \sum_{k=1}^{K} \alpha_k s(t - \tau_k), r(t) - \sum_{k=1}^{K} \alpha_k s(t - \tau_k)\Big)$$

we obtain the condition

$$-2\Big(r(t), s(t - \tau_k)\Big) + 2\Big(s(t - \tau_k), \sum_{n=1}^{K} \alpha_n s(t - \tau_n)\Big) = 0.$$

In other words,

$$\tilde{r}_k = \sum_{k=1}^{K} s_{n,k}\alpha_n, \qquad k = \overline{1, K}, \tag{4.4}$$

where

$$\tilde{r}_k = (r(t), s(t-\tau_k)) = \int r(t)s(t-\tau_k)\,dt.$$

$$s_{n,k} = (s(t-\tau_n), s(t-\tau_k)) = R_s(\tau_k - \tau_n).$$

$R_s(\tau)$is the autocorrelation function.

Equation (4.4) can be written in matrix form

$$\tilde{r} = S\alpha.$$

where $\tilde{r} = (\tilde{r}_1, \ldots, \tilde{r}_K)^T$, $\alpha = (\alpha_1, \ldots, \alpha_K)^T$, $S = \{s_{n,k}\}$. and, therefore, the solution of the minimization problem (4.3) is

$$\alpha = S^{-1}\tilde{r}. \tag{4.5}$$

In engineering terminology, the above is a standard linear quadratic minimization problem. Unfortunately, since the partition $\{\tau_k\}$ is fine, the dimension of the matrix S is large and the solution involves the inversion of a high dimension matrix.

Now, let us assume that the partition $\{\tau_k\}$ is uniform, i.e. $\tau_n - \tau_k = \tau_{n-k}$. and

S is a matrix of Toeplitz type

$$S = \begin{pmatrix} s_0 & s_1 & s_2 & \cdots & s_K \\ s_1 & s_0 & s_1 & \cdots & s_{K-1} \\ s_2 & s_1 & s_0 & \cdots & s_{K-2} \\ \vdots & \vdots & \vdots & \ddots & \vdots \\ s_K & s_{K-1} & s_{K-2} & \cdots & s_0 \end{pmatrix} \tag{4.6}$$

where $s_i = s_{n,n+i} = R_s(\tau_{n+i} - \tau_n) = R_s(\tau_i)$.

Remark. If the autocorrelation function $R_s(\tau)$ is thumbtack, then the matrix S is very close to the identity matrix and, therefore, there is no need to invert it.

Example 1. Consider the sent signal

$$s(t) = Z^{-1}(T_{20}(\cos \pi x \cdot \cos \pi y))(t).$$

which, as was shown in the previous chapter, has a 'thumbtack' ambiguity function

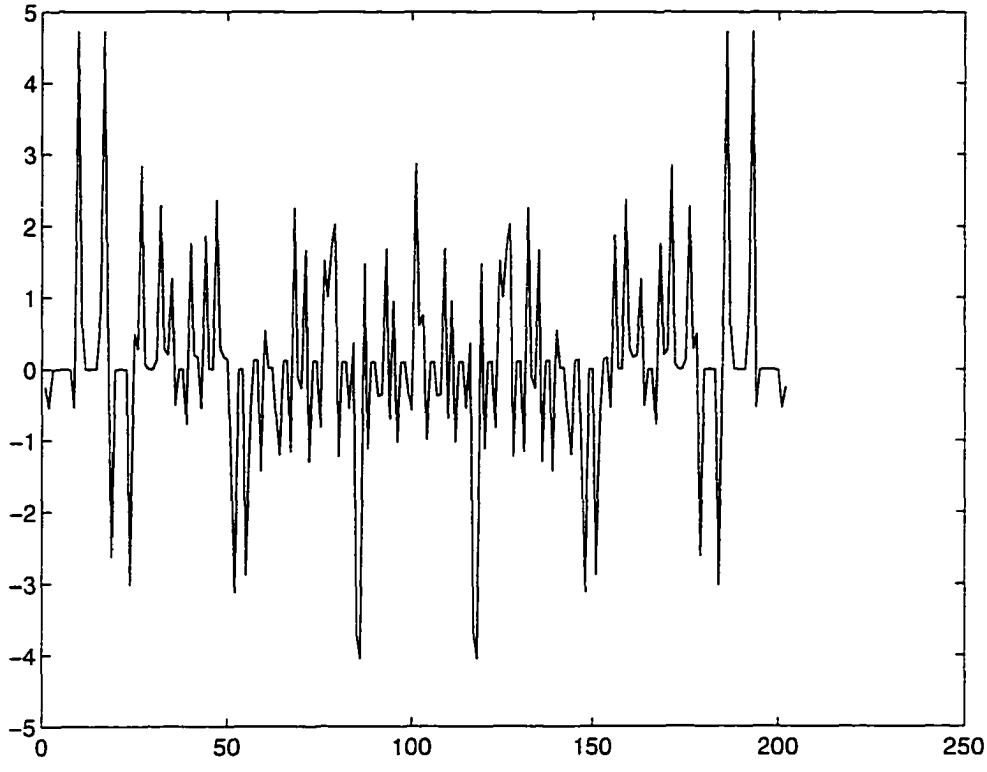

Figure 4.1. Signal based on two-dimensional trigonometric Chebychev polynomial T_{20}.

and the received signal

$$r(t) = s_9(t) + n(t). \qquad n(t) = N(0.3).$$

with signal to noise ratio

$$SNR = 10 \log_{10} \frac{\sum_k |s_9(k)|^2}{3^2} = 8.7527 \, \text{dB}.$$

The vector $\tilde{r} = \{(r(t), s(t - \tau_i))\}$ is shown in figure 4.3 with the true attenuation coefficients α_k marked by an asterisk.

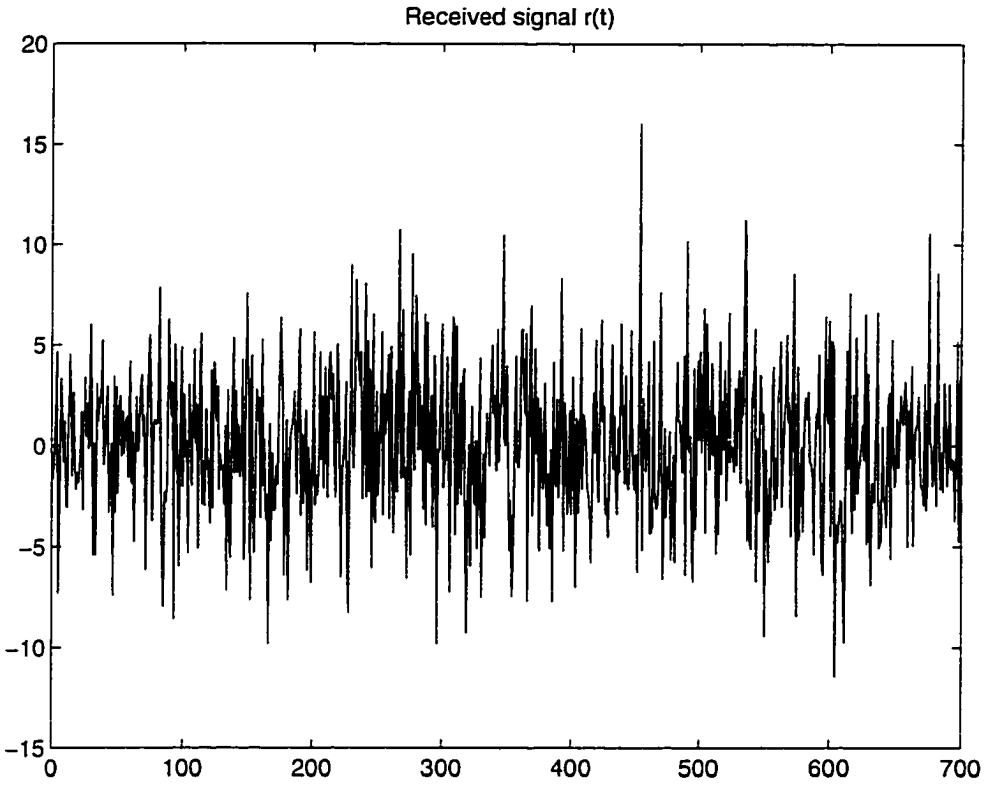

Figure 4.2. Received signal $r(t)$.

Thus, as can be seen from figure 4.3, true delays correspond to the highest peaks of the vector $\tilde{r}$. This happened because of the thumbtack nature of the ambiguity function, since if $S^{-1} \approx I$ then the solution is given by $\alpha \approx \tilde{r}$.

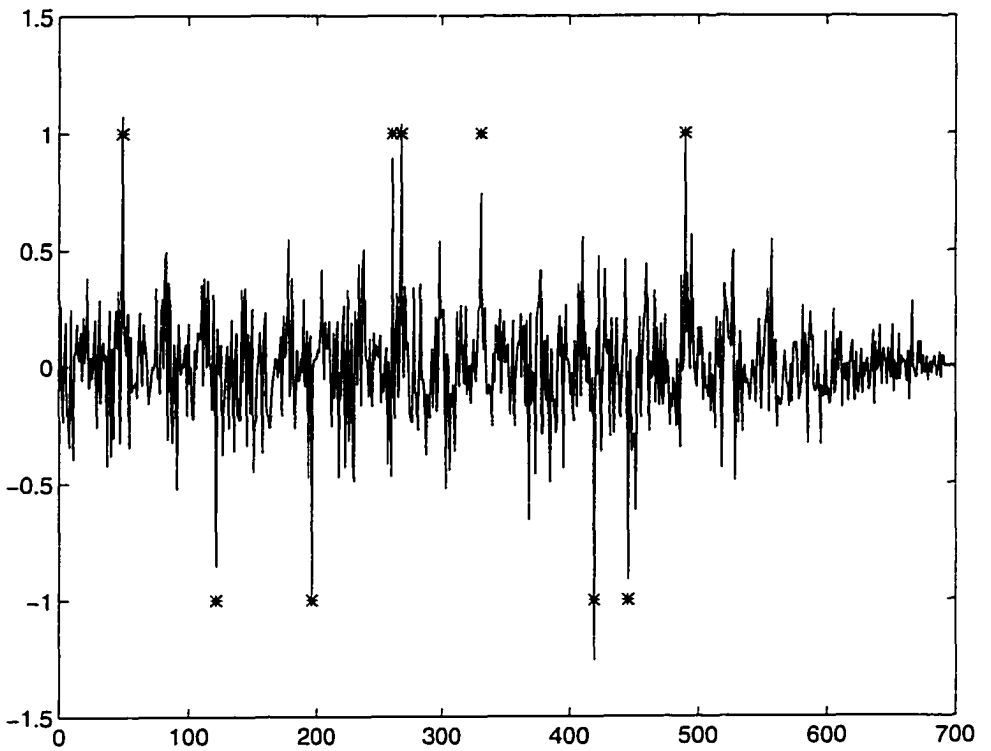

Figure 4.3. Vector $\tilde{r} = \{(r(t).s(t-\tau_i))\}$.

4.2 Matrix approximation

Now, S can be written in the form

$$S = s_0 I + s_1(F + F^{-1}) + s_2(F^2 + F^{-2}) + \ldots + s_{K-1}(F^{K-1} + F^{-(K-1)}). \quad (4.7)$$

where I is the identity matrix, and

$$F^i = \begin{pmatrix} 0 & \dots & 0 & 1 & 0 & \dots & 0 \\ 0 & & & 0 & 1 & \dots & 0 \\ \vdots & & & & & \ddots & \vdots \\ 0 & & & & & & 1 \\ \vdots & & & & & & \vdots \\ 0 & \dots & 0 & 0 & 0 & \dots & 0 \end{pmatrix}$$

with 1's on the i'th diagonal. The matrices F^i have some nice properties:

1. $F^{-i} = (F^i)^T$;
2. i'th power of F^1 is F^i, i.e. $(F^1)^i = F^i$;
3. $(F^{-1})^i = F^{-i}$;
4. F^{-i} is a pseudoinverse of F^i, i.e., $(F^{-i})(F^i)$ is the identity on the orthocomplement of the i-dimensional subspace.

To find S^{-1}, consider the polynomial $\varphi(\lambda)$ corresponding to the matrix equation (4.7):

$$\varphi(\lambda) = s_0 + s_1(\lambda + \lambda^{-1}) + s_2(\lambda^2 + \lambda^{-2}) + \ldots + s_{K-1}(\lambda^{K-1} + \lambda^{-(K-1)}). \quad (4.8)$$

Our goal is to find $G = S^{-1} = [\varphi(F)]^{-1}$. Let us first find $g(\lambda) = [\varphi(\lambda)]^{-1} = \frac{1}{\varphi(\lambda)}$ for a complex variable λ.

To find $g(\lambda)$ we represent $\phi(\lambda)$ as a product

$$\dot{\phi}(\lambda) = s_{K-1}\lambda^{1-K}\prod_{k=0}^{K-1}(\lambda - \lambda_k)(\lambda - \frac{1}{\lambda_k}). \tag{4.9}$$

where the λ_k are the roots of the polynomial $\phi(\lambda)$. Obviously, the $\frac{1}{\lambda_k}$ are also the roots of the polynomial $\phi(\lambda)$.

Let us assume, for simplicity, that all roots of $\phi(\lambda)$ are distinct, i.e. of multiplicity one, and are not equal to 1 in absolute value:

$$|\lambda_1| > |\lambda_2| > \ldots > |\lambda_{K-1}| > 1. \tag{4.10}$$

Then

$$g(\lambda) = \frac{1}{\phi(\lambda)} = \sum_{k=1}^{K}\left[\frac{A_k\lambda_k}{\lambda - \lambda_k} - \frac{A_k\lambda_k^{-1}}{\lambda - \lambda_k^{-1}}\right]. \tag{4.11}$$

where

$$\lambda_k A_k = \lim_{\lambda\to\lambda_k}\frac{\lambda - \lambda_k}{\phi(\lambda)} = \frac{1}{\dot{\phi}(\lambda_k)}.$$

Moreover, since by assumption, all roots are of multiplicity one, the derivative $\dot{\phi}(\lambda_k)$ is not equal to zero.

Equality (4.11) can be rewritten as

$$g(\lambda) = \frac{1}{\phi(\lambda)} = -\sum_{k=1}^{K-1}\left[\frac{A_k}{1 - \lambda_k^{-1}\lambda} + \frac{A_k\lambda^{-1}\lambda_k^{-1}}{1 - \lambda_k^{-1}\lambda^{-1}}\right] =$$

$$= \sum_{k=1}^{K} \left[\sum_{n=0}^{\infty} \lambda^n \lambda_k^{-n} + \sum_{n=1}^{\infty} \lambda^{-n} \lambda_k^{-n} \right] A_k \qquad (4.12)$$

(the series converges since $|\lambda_k| > 1$).

The decomposition (4.12) allows us to hope that

$$G = S^{-1} = [\phi(F)]^{-1} \approx - \sum_{k=1}^{K-1} \left[\sum_{n=0}^{K-1} F^n \lambda_k^{-n} + \sum_{n=1}^{K-1} F^{-n} \lambda_k^{-n} \right] A_k \qquad (4.13)$$

Equality in (4.12) is replaced by approximate equality in (4.13) since F^{-1} is not the inverse matrix of F^1 but the pseudoinverse. The series in (4.12) is replaced by finite sums since F is nilpotent.

To see the character of the approximation (4.13), we consider a spline as a sent signal.

4.3 Spline as a sent signal

Consider a spline $N_m(t)$ of order m, which is recurrently determined by

$$N_m(t) = \int_{-\infty}^{\infty} N_1(x) N_{m-1}(t-x)\, dx, \qquad m > 0.$$

where $N_1(t)$ is a rectangular pulse of duration 1. Then the matrix S is close to the identity matrix and its elements $s_i = N_{2m}(\tau_i - m)$ (see (4.6)) and for $m = 3$

$$S \approx \frac{1}{9}\begin{pmatrix} 5 & 2 & 0 & 0 & 0 \\ 2 & 5 & 2 & 0 & 0 \\ 0 & 2 & 5 & 2 & 0 \\ 0 & 0 & 2 & 5 & 2 \\ 0 & 0 & 0 & 2 & 5 \end{pmatrix}.$$

Here $\phi(\lambda) = \frac{1}{9}(2\lambda^{-1} + 5 + 2\lambda)$ and root $\lambda_1 = -2$. Thus

$$S^{-1} \approx G = \frac{3}{16}\begin{pmatrix} 16 & -8 & 4 & -2 & 1 \\ -8 & 16 & -8 & 4 & -2 \\ 4 & -8 & 16 & -8 & 4 \\ -2 & 4 & -8 & 16 & -8 \\ 1 & -2 & 4 & -8 & 16 \end{pmatrix}.$$

and

$$SG = \begin{pmatrix} 4/3 & -1/6 & 1/12 & -1/24 & 1/48 \\ 0 & 1 & 0 & 0 & 0 \\ 0 & 0 & 1 & 0 & 0 \\ 0 & 0 & 0 & 1 & 0 \\ 1/48 & -1/24 & 1/12 & -1/6 & 4/3 \end{pmatrix} \approx SS^{-1} = I.$$

The first and the last rows in the product SG are different from those in the identity matrix as are the first and the last columns in the product GS. As the dimension of the matrix S increases, this becomes less and less important.

4.4 Pulse as a sent signal

Now we consider an unfavorable example when assumption (4.10) is not satisfied.

For the signal

$$s(t) = \begin{cases} 1. & 0 \le t \le m. \\ 0. & \text{otherwise} \end{cases}$$

the matrix S for $(m = 3)$ is

$$S = \begin{pmatrix} 3 & 2 & 1 & 0 & \dots & \dots & 0 \\ 2 & 3 & 2 & 1 & & & 0 \\ 1 & 2 & 3 & 2 & \ddots & & 0 \\ 0 & \ddots & \ddots & \ddots & \ddots & \ddots & \vdots \\ \vdots & \ddots & \ddots & \ddots & \ddots & \ddots & 1 \\ \vdots & & \ddots & \ddots & \ddots & \ddots & 2 \\ 0 & \dots & \dots & 0 & 1 & 2 & 3 \end{pmatrix}$$

and the characteristic polynomial

$$o(\lambda) = \lambda^{m-1} + 2\lambda^{m-2} + \ldots + (m-1)\lambda + m + \frac{m-1}{\lambda} + \ldots + \frac{2}{\lambda^{m-2}} + \frac{1}{\lambda^{m-1}}$$

can be written in the form

$$o(\lambda) = \lambda^{-(m-1)}(\lambda^{m-1} + \lambda^{m-2} + \ldots + 1)^2 = \lambda^{1-m}\left(\frac{1-\lambda^m}{1-\lambda}\right)^2.$$

The roots of this polynomial $\lambda_k = e^{\frac{2\pi ik}{m}}$ are all of multiplicity two and in absolute value equal one. Thus the series in (4.12) fail to converge and the

decomposition (4.11) for multiple roots has a different form to begin with.

Let us find $g(\lambda)$:

$$g(\lambda) = \frac{1}{\phi(\lambda)} = \lambda^{m-1}\frac{1-\lambda}{1-\lambda^m}\cdot\frac{1-\lambda}{1-\lambda^m} = \frac{1-\lambda^{-1}}{1-\lambda^{-m}}\cdot\frac{1-\lambda}{1-\lambda^m} =$$

$$= (1-\lambda^{-1})(1-\lambda^m+1-\lambda^{-m})^{-1}(1-\lambda). \qquad (4.14)$$

The decomposition (4.14) allows us to expect that

$$S^{-1} = [\phi(F)]^{-1} \approx (I-F^{-1})\left[(I-F^m)+(I-F^{-m})\right]^{-1}(I-F) \qquad (4.15)$$

To investigate the character of the approximation (4.15) we need some preliminaries. For details see [14].

Definition 1. The distance between matrices A and B is defined as the rank of their difference.

Definition 2. The matrix A is *close* to matrix B if the distance between them is small.

Lemma. For non-singular matrices A and B, if A is close to B, then A^{-1} is close to B^{-1}, cf. [14].

Now we can prove the following theorem.

Theorem 4.1. Let $A = (I-F)\cdot S\cdot(I-F^{-1})$ and $B = (I-F^m)+(I-F^{-m})$, then A is close to B.

Proof. We rewrite S as

$$S = \sum_{k=1}^{m} kF^{m-k} + \sum_{k=1}^{m} kF^{-1(m-k)} - mI \tag{4.17}$$

and consider $A = (I - F) \cdot S \cdot (I - F^{-1})$.

After simple algebraic manipulations (see Appendix A), we obtain

$$A = (I - F^m) + (I - F^{-m}) +$$

$$+(FF^{-1} - I) \sum_{k=0}^{m-1} F^{-k} + \sum_{k=0}^{m-1} F^k (FF^{-1} - I) + m(I - FF^{-1}). \tag{4.18}$$

The rank of the sum of the last three terms is two, therefore A is close to B.

Remark 1. The purpose of this theorem is to show the character of the approximate equality (4.15). Since

$$A^{-1} = [(I - F) \cdot S \cdot (I - F^{-1})]^{-1} = (I - F^{-1})^{-1} S^{-1} (I - F)^{-1},$$

we have

$$S^{-1} = (I - F^{-1}) A^{-1} (I - F).$$

Since A is close to B, then, by the Lemma, A^{-1} is close to B^{-1} and thus we have

$$S^{-1} \approx (I - F^{-1})[(I - F^m) + (I - F^{-m})]^{-1} (I - F).$$

The structure of the matrix S^{-1} is shown on the figures (4.4) and (4.5). We have

indicated the structure in the form of a 3-dimensional graph of the matrix values.

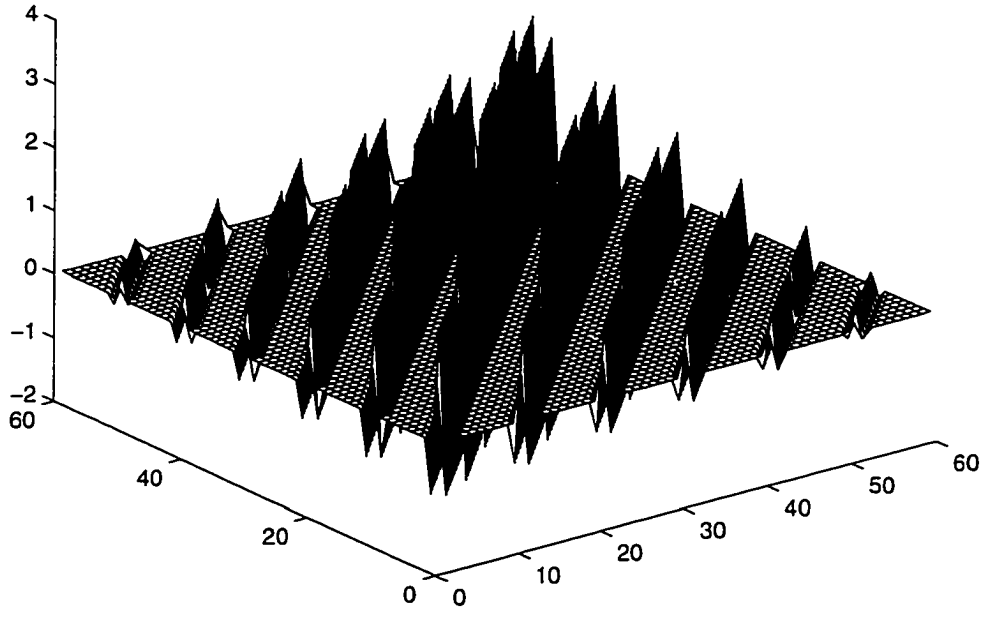

Figure 4.4. Structure of the matrix S^{-1} with $m = 10$ and $K = 60$.

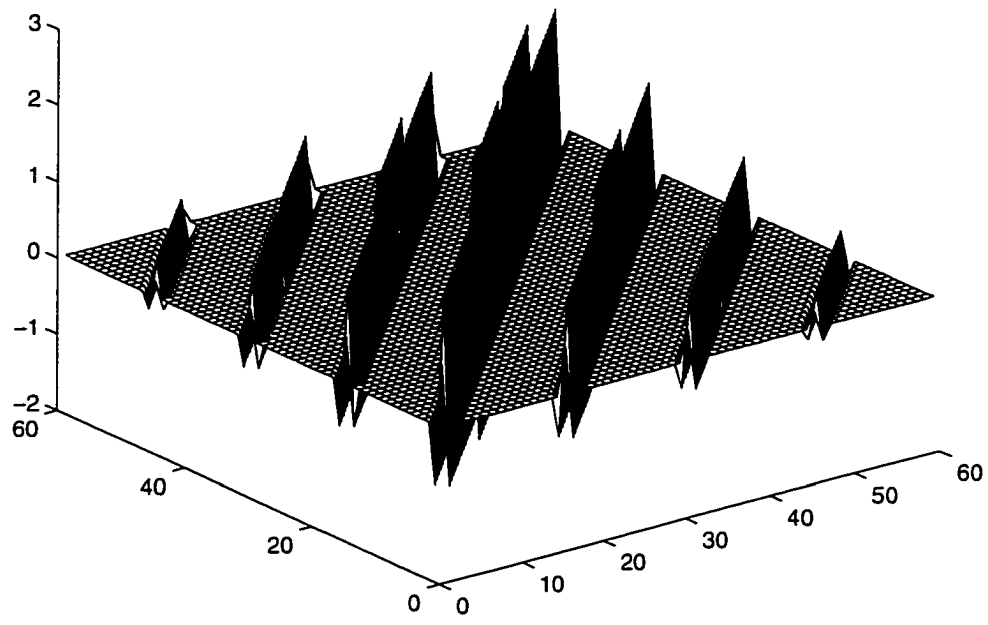

Figure 4.5. Structure of the matrix S^{-1} with $m = 15$ and $K = 60$.

Remark 2. In this case, as can be seen from figures (4.4), (4.5) and from the approximate equality (4.15), the longer the pulse $s(t)$ the better the matrix S^{-1} in terms of memory requirements. In the extreme situation, when $m = K$

$$S^{-1} \approx \frac{1}{2}(I - F^{-1})(I - F),$$

therefore

$$\alpha \approx S^{-1}\tilde{r} = \frac{1}{2}(I - F^{-1})(I - F)\tilde{r}$$

thus α is nothing but a finite difference second derivative of $\tilde{r}$.

Recall that $\tilde{r}$ is a scalar product of the received signal $s_K(t) + n(t)$ (see figure 4.6) with shifted versions of the sent signal $s(t)$, and since $n(t)$ is highly oscillatory, so is $\tilde{r}$.

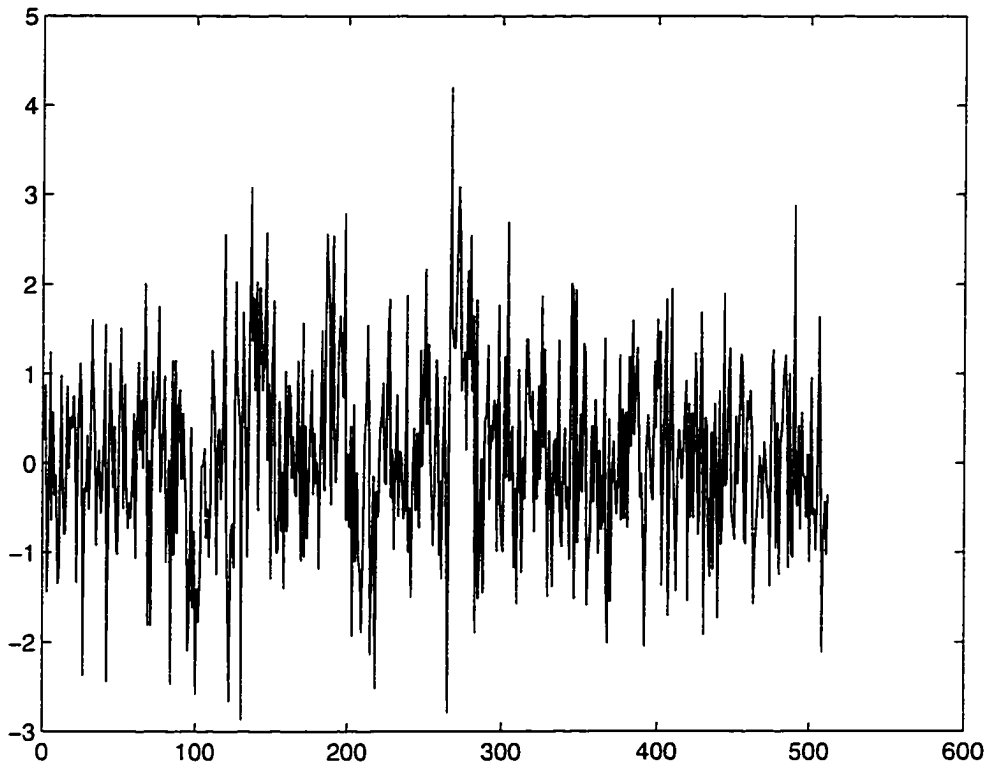

Figure 4.6. Received signal $r(t) = s_4(t) + n(t)$.

Therefore our solution $\alpha = S^{-1}\tilde{r} \approx (I - F^{-1})A^{-1}(I - F)\tilde{r}$ is based on computations of the (difference) derivatives of $\tilde{r}$. That is why the solution α (see figure 4.7) will be highly oscillatory.

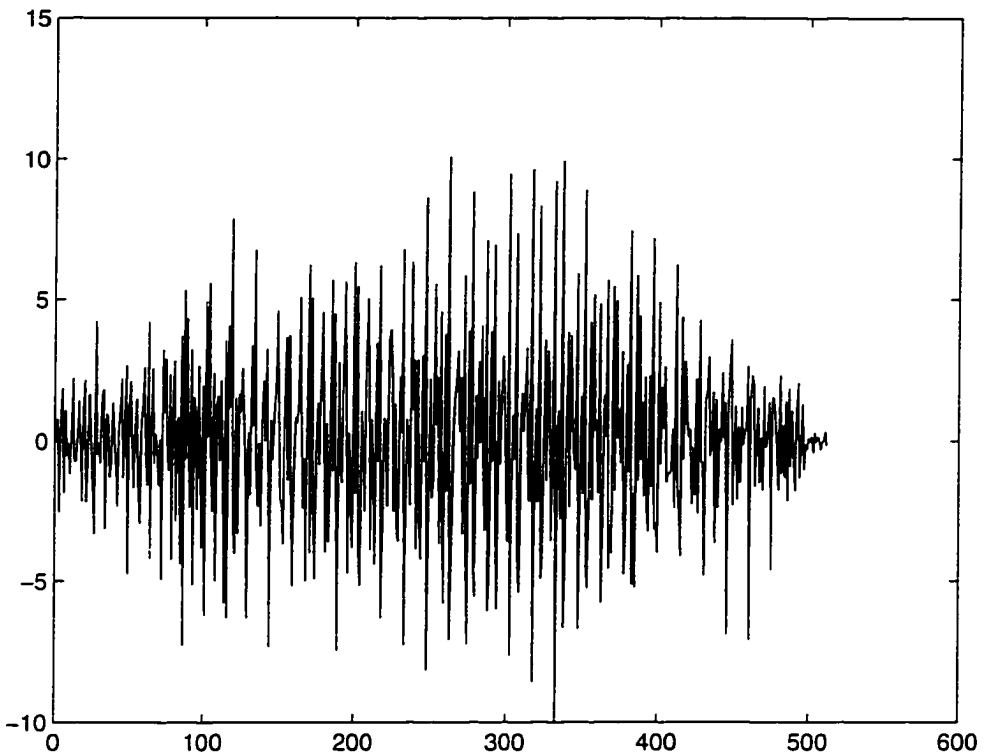

Figure 4.7. Attenuation coefficients $\alpha = S^{-1}\tilde{r}$.

If we compare the computed attenuation coefficients α with the true coefficients (figure 4.8), we see a dramatic difference. However, the problem in this approach is the following: for a very large number of possible delays, the sum

$$s_K(t) = \sum_{k=1}^{K} \alpha_k s(t - \tau_k)$$

(see figure 4.9)

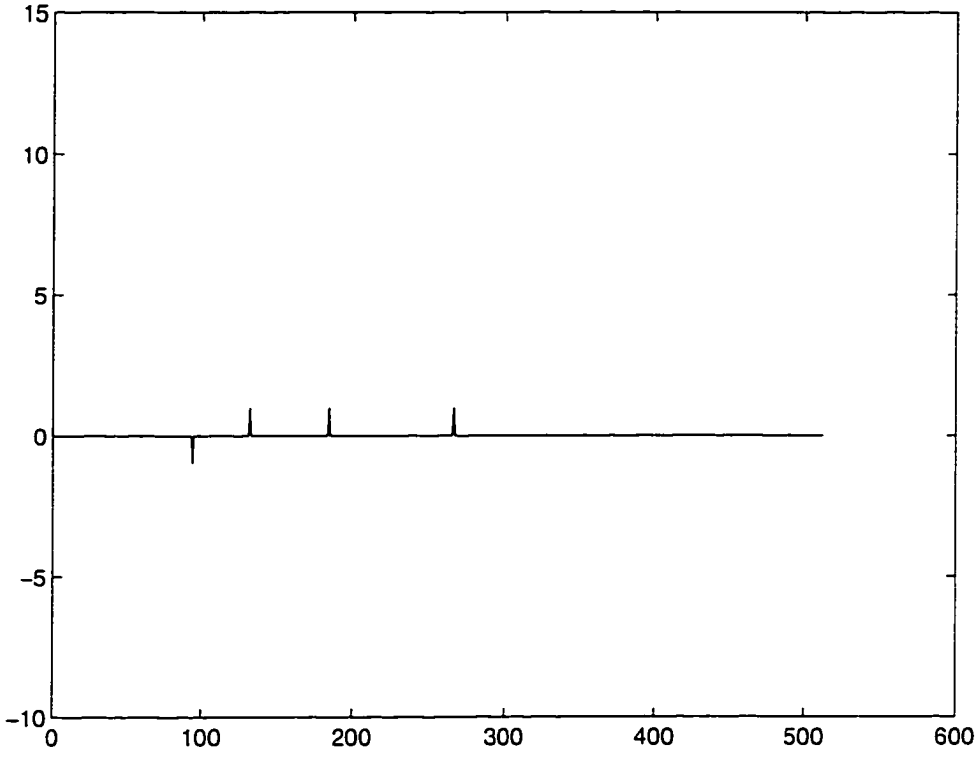

Figure 4.8. True attenuation coefficients a.

is very close to the received signal $r(t)$ (it is almost impossible to tell figure 4.6 and 4.8 apart), so that the distance

$$\|r(t) - s_K(t)\|_{L^2} = \|n(t)\| \tag{4.19}$$

is almost zero (it is equal to 0.0195 in this particular example). In other words, for a very large number K of delays, the very large number of degres of freedom enable an almost perfect match of $r(t)$ by $s_K(t)$.

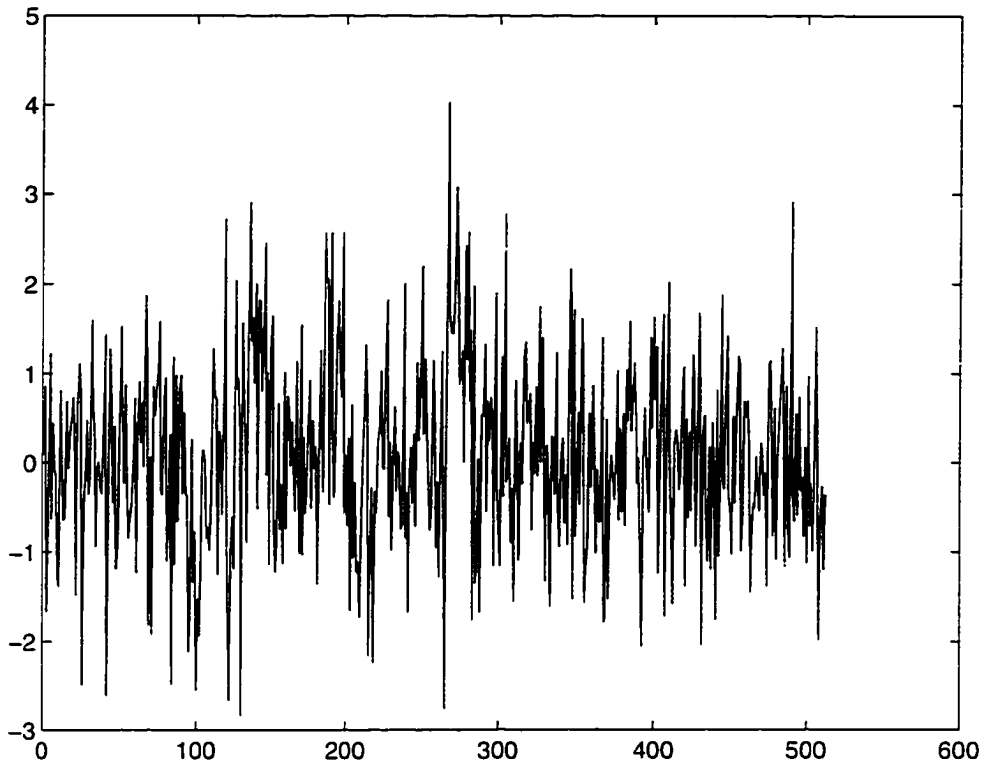

Figure 4.9. The sum $s_K(t)$ with the coefficients $\alpha = S^{-1}\tilde{r}$.

This is not a contradiction of any kind, we were solving the problem

$$\min_{r_k,\alpha_k,K} \|r(t) - s_K(t)\|_{L^2} \tag{4.20}$$

and we found a way to drive this distance to zero. The difference $r(t) - s_K(t)$ is shown on figure 4.10. To avoid this problem, we could change the cost function by adding a term dependent on the number of degrees of freedom K. In what follows, we will take a somewhat different approach. (cf. the remarks in the Introduction).

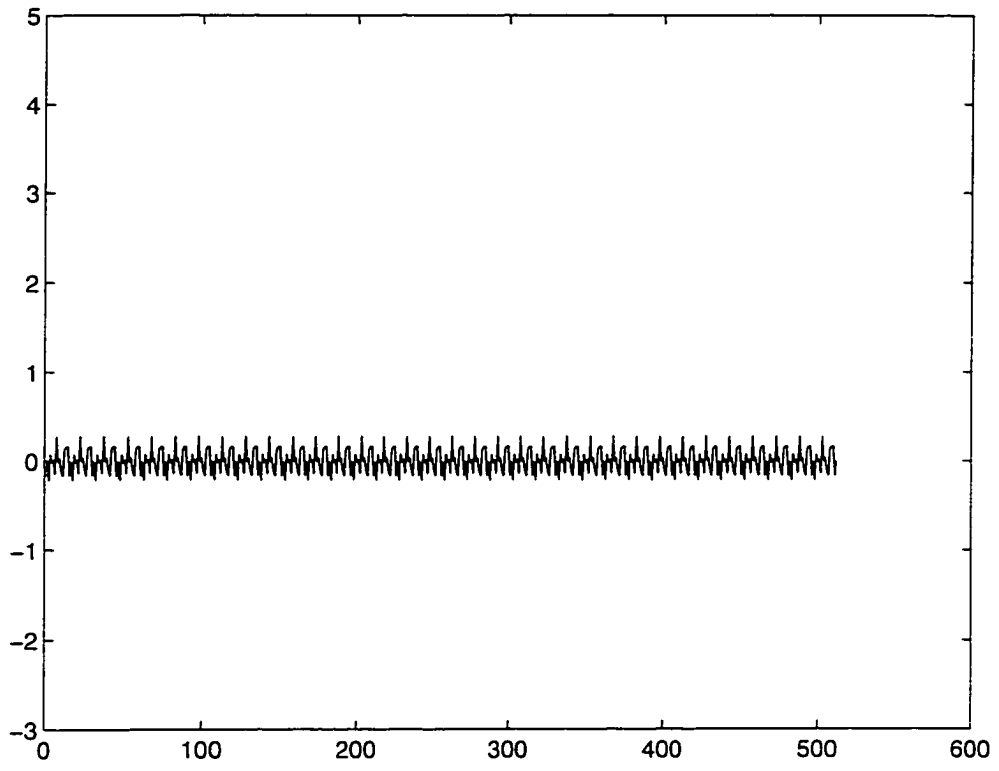

Figure 4.10. The difference $r(t) - s_K(t)$.

This problem is taken care of here with a high frequency cutoff Fourier transform technique, as shown in the next section.

4.5 Continuous case

Let us rewrite equation (4.1) in the continuous case, i.e. when τ_k is a variable on the interval (T_0, T_1):

$$s_K(t) = \int_{T_0}^{T_1} \alpha(\tau) s(t-\tau)\, dt = (\alpha * s)(t) \tag{4.21}$$

and

$$r(t) = s_K(t) + n(t) = (\alpha * s)(t) + n(t). \tag{4.22}$$

Then

$$FT(r) = FT(\alpha) \cdot FT(s) + FT(n).$$

where $FT(r)$ is a Fourier transform of $r(t)$.

Thus, the attenuation coefficients can be found with an inverse Fourier transform:

$$\alpha = FT^{-1}\big[(FT(r) - FT(n))/FT(s)\big]. \tag{4.23}$$

As we said before, this approach of increasing the dimension of the original minimization problem drives the distance (4.19) to zero, which corresponds to a very small noise $n(t)$, and $FT(n)$ in (4.23) can be ignored (it is not available at the receiver anyway). And, as we pointed out earlier, the solution $\alpha = S^{-1} \cdot \tilde{r}$ (in the discrete case) or $\alpha = FT^{-1}\big[FT(r)/FT(s)\big]$ (in the continuous case) is a very oscillatory function. To reduce this oscillation, we will chop off the big frequencies before taking the inverse Fourier transform. It turns out that this method produces satisfactory results.

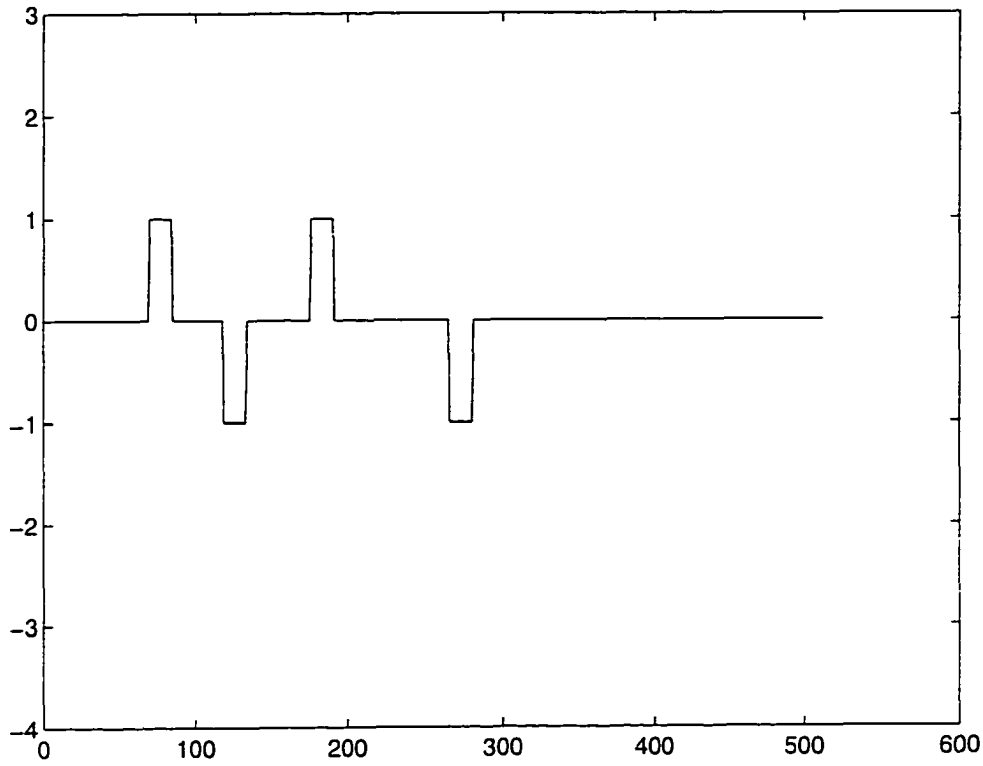

Figure 4.11. True multipath signal $s_4(t)$.

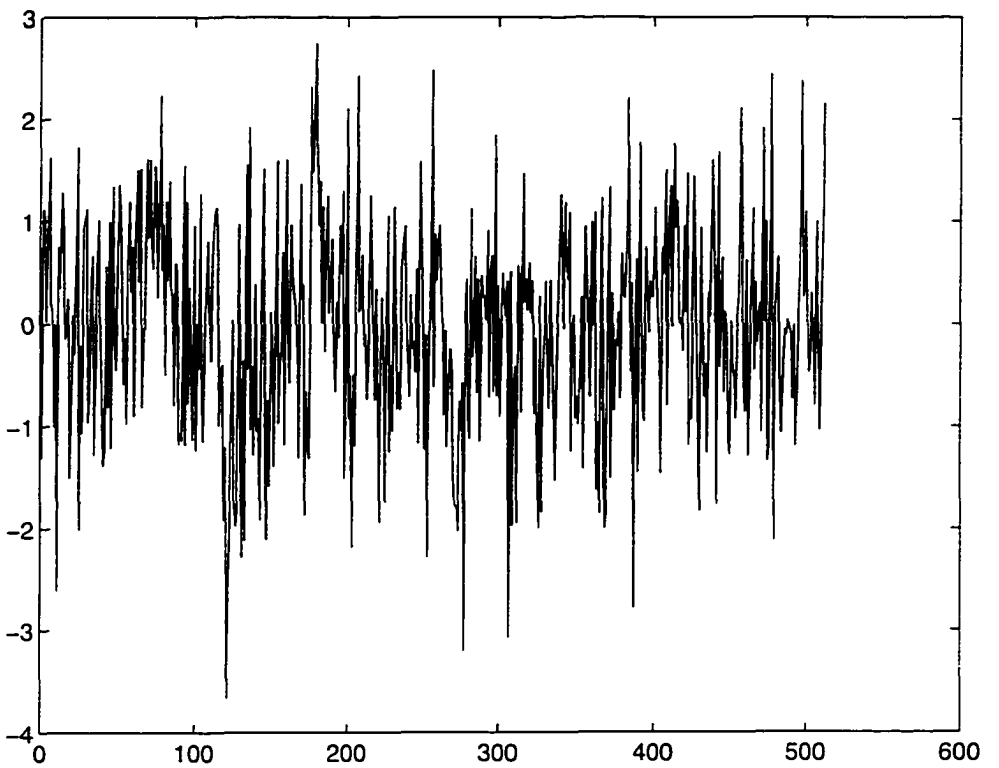

Figure 4.12. Received signal $r(t) = s_1(t) + n(t)$.

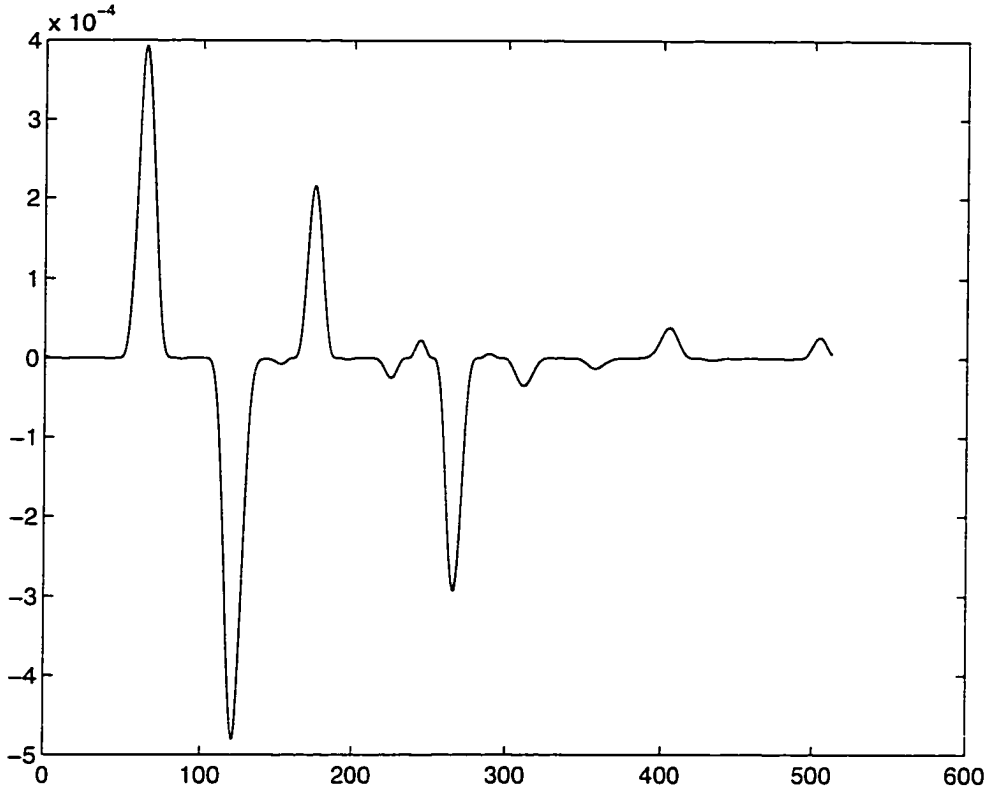

Figure 4.13. 'Smoothed out' attenuation coefficients, found with our new method.

Appendix A

Proof of the identity (4.18)

$$(I-F)S=\sum_{k=1}^{m}kF^{m-k}+\sum_{k=1}^{m}kF^{-(m-k)}-mI-\sum_{k=1}^{m}kF^{m-k+1}-$$

$$-\sum_{k=1}^{m}kFF^{-(m-k)}+mF.$$

Note that

$$\sum_{k=1}^{m}kF^{m-k}-mI-\sum_{k=1}^{m}kF^{m-k+1}=-\sum_{k=1}^{m}F^{k}.$$

$$\sum_{k=1}^{m}kF^{-(m-k)}-\sum_{k=1}^{m}kFF^{-(m-k)}+mF=\sum_{k=0}^{m-1}F^{-k}+(I-FF^{-1})\sum_{k=1}^{m-1}kF^{-(m-k-1)}.$$

where the last term in the right-hand side is the matrix of a rank 1. It consists of zeros except the last row. Thus

$$(I-F)S=\sum_{k=0}^{m-1}F^{-k}-\sum_{k=1}^{m}F^{k}+(I-FF^{-1})\sum_{k=1}^{m-1}kF^{-(m-k-1)}.$$

Now,

$$A = (I - F)S(I - F^{-1}) = \sum_{k=0}^{m-1} F^{-k} - \sum_{k=1}^{m} F^{k} + (I - FF^{-1}) \sum_{k=1}^{m-1} kF^{-(m-k-1)} -$$

$$- \sum_{k=1}^{m} F^{-k} + \sum_{k=1}^{m} F^{k}F^{-k} - (I - FF^{-1}) \sum_{k=1}^{m-1} kF^{-(m-k)}.$$

Since

$$\sum_{k=0}^{m-1} F^{-k} - \sum_{k=1}^{m} F^{-k} = I - F^{-m};$$

and

$$- \sum_{k=1}^{m} F^{k} + \sum_{k=1}^{m} F^{k}F^{-1} = I - F^{m} - \sum_{k=0}^{m} F^{k}(I - FF^{-1}).$$

where $\sum F^{k}(I - FF^{-1})$ is a matrix of rank 1, consisting of zeros except the last column, then

$$A = (I - F^{m}) + (I - F^{-m}) +$$

$$+ (I - FF^{-1})\Big(\sum_{k=1}^{m-1} kF^{-(m-k-1)} - \sum_{k=1}^{m-1} kF^{-(m-k)}\Big) - \sum_{k=0}^{m-1} F^{k}(I - FF^{-1}) =$$

$$= (I - F^{m}) + (I - F^{-m}) +$$

$$+ \underbrace{(I - FF^{-1})\Big((m-1)I - \sum_{k=1}^{m-1} F^{-k}\Big)}_{\text{last row}} - \underbrace{\sum_{k=0}^{m-1} F^{k}(I - FF^{-1})}_{\text{last column}} =$$

$$= (I - F^{m}) + (I - F^{-m}) +$$

$$+(FF^{-1}-I)\sum_{k=0}^{m-1}F^{-k}+\sum_{k=0}^{m-1}F^{k}(FF^{-1}-I)+m(I-FF^{-1}).$$

Appendix B

Two-dimensional trigonometric Chebyshev polynomials that we need for the theorem 3.1 can also be generated in the following way:

$$\begin{aligned} C_{2^1}(x,y) &= (C_{2^0}(x,y) - c_{2^0})^2 \\ C_{2^2}(x,y) &= (C_{2^1}(x,y) - C_{2^1}(1/2,1/2)^2 \\ &\vdots \\ C_{2^k}(x,y) &= (C_{2^{k-1}}(x,y) - C_{2^{k-1}}(1/2,1/2))^2 \end{aligned}$$

where $C_{2^0}(x,y)$ is an appropriately chosen trigonometric polynomial and c_{2^0} is a parameter.

Example 1. Consider

$$C_{2^0}(x,y) = \cos(2\pi(x+y)) + \cos(2\pi(x-y)) + \cos(2\pi x) + \cos(2\pi y)$$

Polynomial $C_{24}(x, y)$ with $c_{20} = -0.98$ which provides $\varepsilon_1 \approx 0.12$ and $\varepsilon_2 \approx 0.15$ (see theorem 3.1) is shown on figure B.1. The signal corresponding to this polynomial is shown in figure B.2. The ambiguity on the integer lattice is shown in figure B.3.

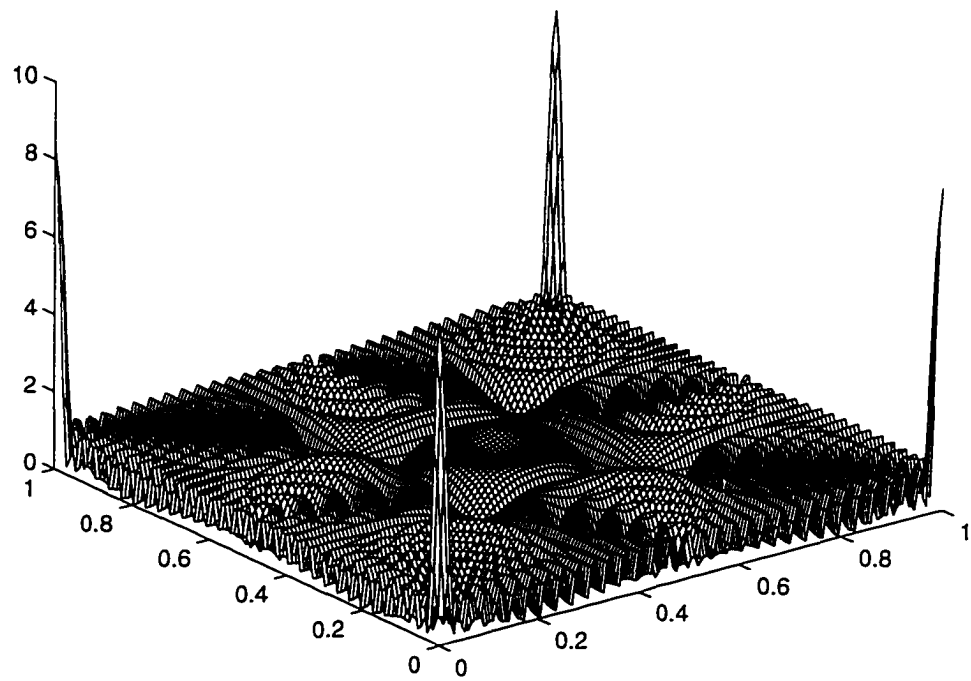

Figure B.1 Polynomial $C_{24}(x, y)$.

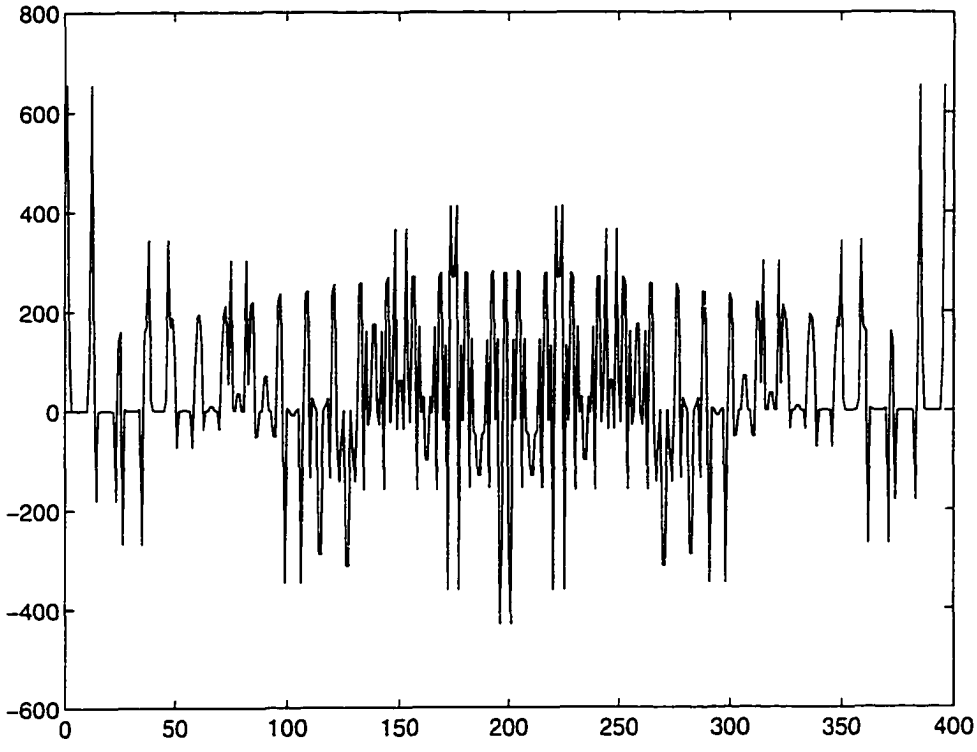

Figure B.2 Signal $s(t) = Z^{-1}(C_{2^3})$.

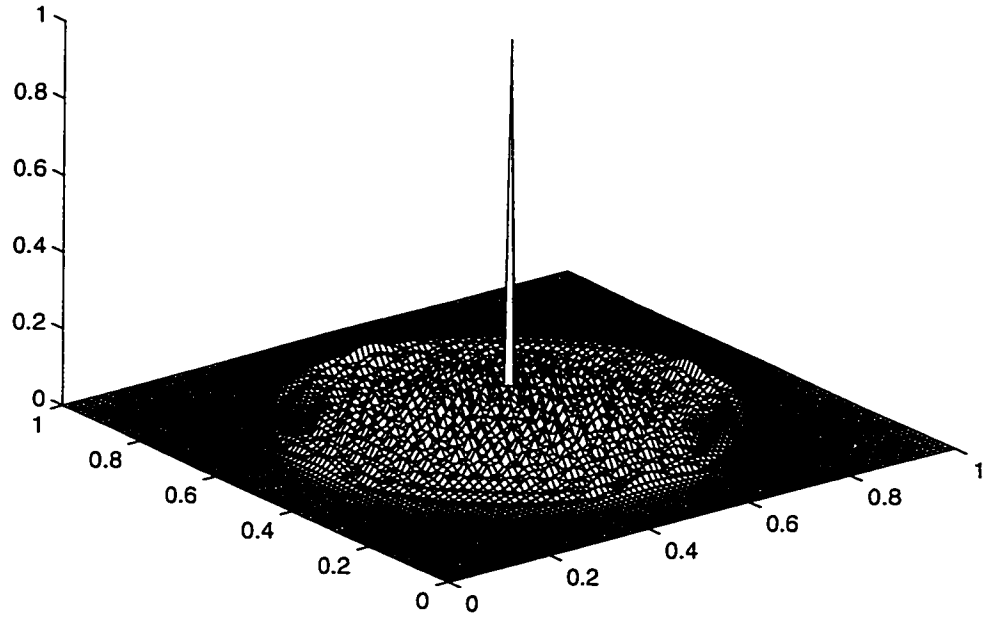

Figure B.3 Ambiguity on the integer lattice.

Example 2. Consider

$$C_{2^0}(x, y) = \cos(2\pi(x + y)) + \cos(2\pi(x - y)).$$

The polynomial $C_{2^4}(x, y)$ with $c_{2^0} = 0.01$ is shown in figure B.6. The signal corresponding to this polynomial is shown in figure B.7. The ambiguity on the integer lattice is shown in figure B.8.

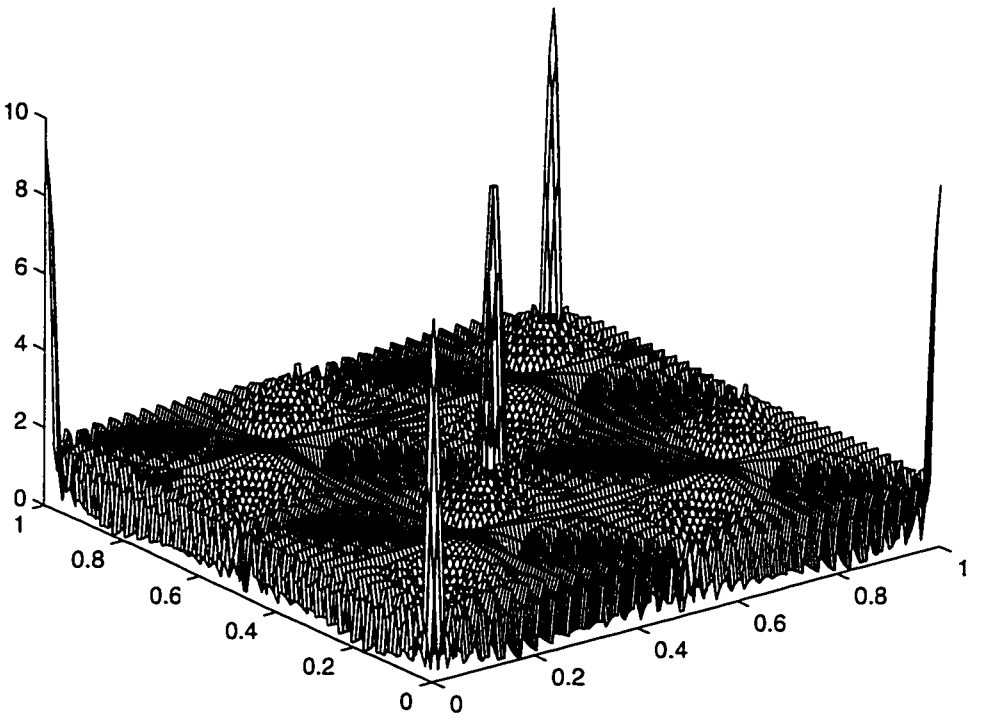

Figure B.4 Polynomial $C_{24}(x, y)$.

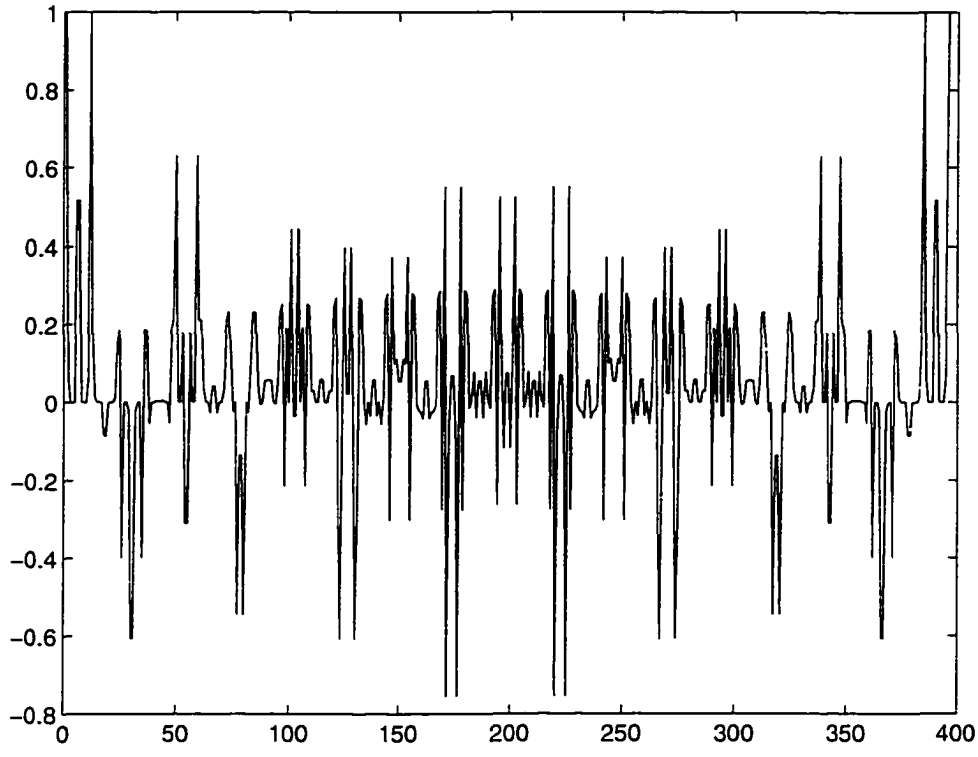

Figure B.5 Signal $s(t) = Z^{-1}(C_{2^3})$.

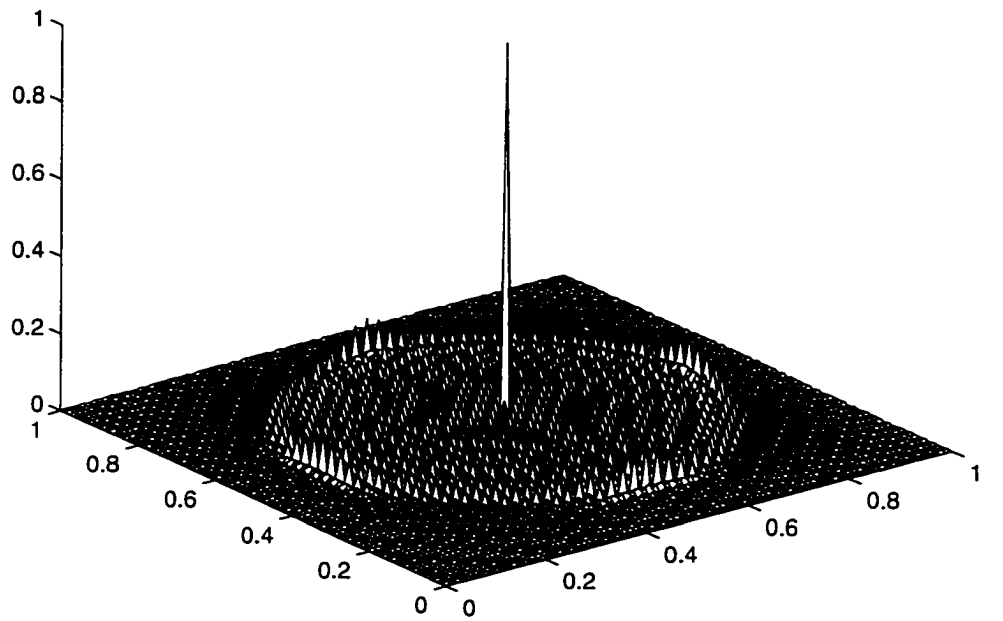

Figure B.6 Ambiguity on the integer lattice.

Bibliography

[1] N.I. ACHIESER. *Theory of Approximation.* Unger, 1956.

[2] L. AUSLANDER, I. GERTNER, & R. TOLIMIERI. The discrete Zak transform application to time-frequency analysis and sythesis of non-stationary signals. *IEEE Trans. Sig. Proc.* **39** (1991), 825–835.

[3] L. AUSLANDER, F. GESHWIND, & F. WARNER. Radar waveform design and the Heisenberg group. *Applied and Computational Harmonic Analysis* **2** (1995), 350–362.

[4] L. AUSLANDER & R. TOLIMIERI. Radar ambiguity functions and group theory. *SIAM J. Math. Anal.* **16** (1985), 577–601.

[5] L. AUSLANDER & F. WARNER. Signal shaping for communication systems. *preprint* .

[6] STEVEN A. BENNO. Robust representations. *Ph.D. Thesis, Carnegie Mellon University* .

[7] STEVEN A. BENNO & JOSÉ M. F. MOURA. On translation invariant subspaces and critically sampled wavelet transforms. *Multidimensional Systems and Signal Processing* **8** (1997), 89–110.

[8] R.E. BLAHUT. *Radar and Sonar, Part I*, chapter Theory of Remote Surveillance Algorithms. Springer-Verlag, 1991.

[9] J.P. COSTAS. A study of a class of detection waveforms having nearly ideal range-doppler ambiguity properties. *Proceedings of the IEEE* **72** (1984), 996–1009.

[10] S. GOLUMB & H. TAYLOR. Construction and properties of Costas arrays. *Proceedings of the IEEE* **72** (1984), 1143–1163.

[11] S.W. GOLUMB. Algebraic constructions for Costas arrays. *J. of Combinatorial Theory* **37** (1984), 13–21.

[12] CHUANG HE. Robust detection: a geometric approach. *Ph.D. Thesis, Carnegie Mellon University*.

[13] A.J.E.M. JANSSEN. The Zak transform: A signal transform for sampled time-continuous signals. *Philips Journal of Research* **43** #43 (1988), 23–69.

[14] G.D. KIM. *Mathematical Encyclopedia*, **4**, chapter Okaymlenia Metod (Russian). Moscow: Soviet Encyclopedia, 1984.

[15] R.M. MERSEREAU & T.S. SEAY. Multiple access frequency hopping patterns with low ambiguity. *IEEE Trans. on Aerospace and Electronic Systems* **AES-17** #4 (1981), 571–578.

[16] T.S. RAPPAPORT. *Wireless Communications: Principles and Practice.* Prentice Hall, 1996.

[17] W.M. SIEBERT. A radar detection philosophy. *IRE Trans. Inform. Theory* **IT-2** (1956), 204–221.

[18] _____. Studies of woodward's ambiguity uncertainty function. *MIT Quarterly Prog. Rep.* (1958), 90–94.

[19] M.I. SKOLNIC. *Introduction to Radar Systems.* McGraw Hill, 1980.

[20] C.A. STUTT. Some results on real-part imaginary-part and magnitude-phase relations on ambiguity functions. *IEEE Trans. Inform.Theory* **IT-20** (1964).

[21] S.M. SUSSMAN. Least-square synthesis of radar ambiguity functions. *IEEE Trans. Inform.Theory* **IT-3** (1962), 246–254.

[22] C.H. WILCOX. The synthesis problem for radar ambiguity functions. *Univ. of Wisconsin MRC Technical Summary Report* #157 (1960).

[23] P. WOODWARD. *Probability and Information Theory, with Applications to Radar.* Pergamon Press, 1953.

IMAGE EVALUATION TEST TARGET (QA-3)

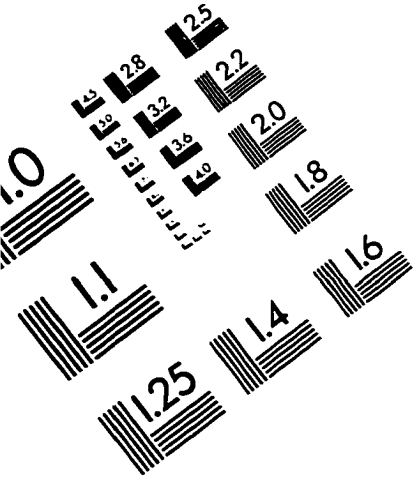

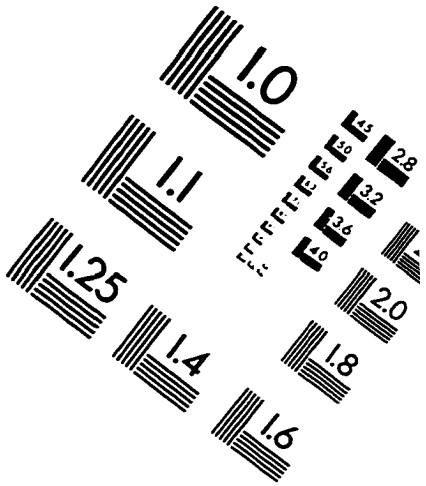

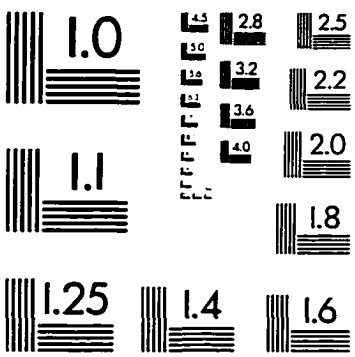

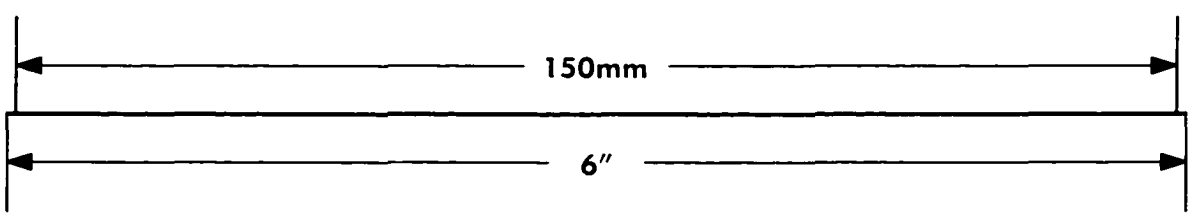

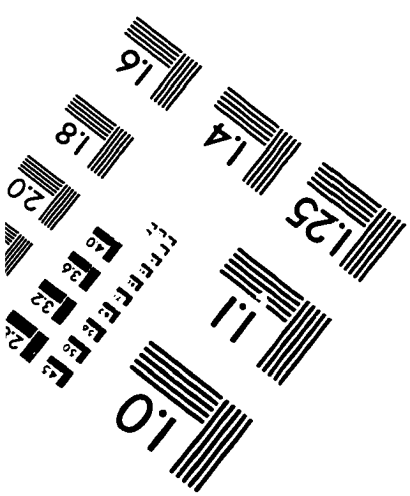

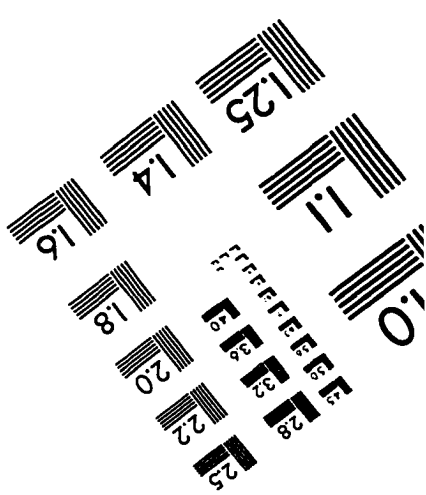

APPLIED IMAGE, Inc
1653 East Main Street
Rochester, NY 14609 USA
Phone: 716/482-0300
Fax: 716/288-5989